

Lawrence Berkeley National Laboratory

Recent Work

Title

MEASUREMENTS OK PROTON-PROTON SCATTERING IN THE ENERGY REGION 150 TO 340 MEV

Permalink

<https://escholarship.org/uc/item/38h8b5s6>

Author

Pettengill, Gordon H.

Publication Date

1954-12-06

UCRL—2808
UNCLASSIFIED

UNIVERSITY OF
CALIFORNIA

*Radiation
Laboratory*

TWO-WEEK LOAN COPY

*This is a Library Circulating Copy
which may be borrowed for two weeks.
For a personal retention copy, call
Tech. Info. Division, Ext. 5545*

BERKELEY, CALIFORNIA

DISCLAIMER

This document was prepared as an account of work sponsored by the United States Government. While this document is believed to contain correct information, neither the United States Government nor any agency thereof, nor the Regents of the University of California, nor any of their employees, makes any warranty, express or implied, or assumes any legal responsibility for the accuracy, completeness, or usefulness of any information, apparatus, product, or process disclosed, or represents that its use would not infringe privately owned rights. Reference herein to any specific commercial product, process, or service by its trade name, trademark, manufacturer, or otherwise, does not necessarily constitute or imply its endorsement, recommendation, or favoring by the United States Government or any agency thereof, or the Regents of the University of California. The views and opinions of authors expressed herein do not necessarily state or reflect those of the United States Government or any agency thereof or the Regents of the University of California.

UCRL-2808
Unclassified Physics

UNIVERSITY OF CALIFORNIA

Radiation Laboratory
Berkeley, California

Contract No. W-7405-eng-48

MEASUREMENTS ON PROTON-PROTON SCATTERING
IN THE ENERGY REGION 150 TO 340 MEV

Gordon H. Pettengill
(Thesis)

December 6, 1954

Printed for the U. S. Atomic Energy Commission

MEASUREMENTS ON PROTON-PROTON SCATTERING
IN THE ENERGY REGION 150 TO 340 MEV

Contents

| | |
|--|----|
| Abstract. | 4 |
| I Introduction | 5 |
| II Small-Angle Experiment | |
| A. Experimental Design | 7 |
| 1) General | |
| 2) Target | |
| 3) Geometry and Counters | |
| 4) Electronics | |
| B. Procedure. | 22 |
| 1) Line-up | |
| 2) Delays and Plateaus | |
| 3) Range Curves and Alignment Checks | |
| 4) Taking Data | |
| C. Data Reduction and Errors | 26 |
| 1) Cross Section Calculations | |
| 2) Polarization Calculations | |
| III Attenuation Experiment | |
| A. Method. | 36 |
| 1) General Description and Layout | |
| 2) Collimation and Energy Reduction | |
| 3) Target and Counters | |
| 4) Electronic and Photographic Set-up | |
| B. Procedure. | 41 |
| 1) Line-up | |
| 2) Range Curves and Beam Homogeneity | |
| 3) Taking Data | |
| C. Data Reduction and Errors | 47 |
| 1) Reading the Film | |
| 2) Calculations | |
| 3) Corrections | |
| 4) Errors | |

| | | |
|----|--|----|
| IV | Discussion | |
| | A. Small-Angle Cross Section | 55 |
| | B. Small-Angle Polarization | 57 |
| | C. Attenuation Cross Section and the Charge-independent Inequality. | 60 |
| V | Conclusion | 63 |
| VI | Acknowledgments | 64 |
| | Appendices | 65 |
| | A. Pile-up and Accidentals | |
| | B. Small-Angle Scattering Geometry | |
| | C. Angular Resolution | |
| | D. Asymmetry for Counter of Finite Extent | |
| | E. Error in Asymmetry Due to Misalignment | |
| | F. Geometry for Attenuation Experiment | |
| | References | 70 |

MEASUREMENT ON PROTON-PROTON SCATTERING
IN THE ENERGY REGION 150 TO 340 MEV

Gordon H. Pettengill
(Thesis)

Radiation Laboratory, Department of Physics
University of California, Berkeley, California

December 6, 1954

ABSTRACT

The 300-Mev proton-proton differential scattering cross section and polarization have been measured for center-of-mass scattering angles between 6.5° and 21.7° . Measurements of the integrated differential proton-proton cross section for angles between 20° and 90° center-of-mass have also been carried out by measurement of attenuation in liquid hydrogen at mean energies of 160, 230, and 330 Mev. In both sets of experiments the incident beam was counted directly. An indication of destructive interference was noted in the small-angle region where Rutherford and purely nuclear effects are comparable. The attenuation measurements give a value of cross section in agreement with previous work at this laboratory. The hypothesis of charge-independent nuclear forces seems not to be violated.

MEASUREMENTS ON PROTON-PROTON SCATTERING
IN THE ENERGY REGION 150 TO 340 MEV

Gordon H. Pettengill
(Thesis)

Radiation Laboratory, Department of Physics
University of California, Berkeley, California

December 6, 1954

I. INTRODUCTION

There has accumulated in the last few years considerable experimental literature¹⁻¹¹ on the subject of proton-proton scattering in the energy region 100 to 400 Mev. Theoretical attempts¹¹⁻²² to fit data in this energy region with the results of low-energy experiments have met with only limited success, particularly if charge-independent interaction potentials are assumed, and agreement with high-energy neutron-proton scattering is demanded.

In the present difficult situation, a few certainties stand out. Despite its simple, almost constant angular distribution, the magnitude of the proton-proton scattering cross section in this energy region requires contributions from partial waves with angular momenta higher than zero.¹ This same expected conclusion must be drawn from the forward-peaked aspect of recent high-energy proton-proton polarization data.²³⁻²⁷ In fact, the hope of determining the degree to which the higher-order partial waves are present led to the inclusion of polarization in the small-angle program presented here in Chapter II and discussed in Chapter IV.

The behavior of the proton-proton cross sections in the small-angle region, where interference between Rutherford and purely nuclear scattering becomes important, has been of recent interest.^{18, 21} Here information is sought to permit a selection between self-consistent groups of phase shifts determined from the larger-angle, purely nuclear scattering data. The experimental data obtained in Chapter II round out the earlier work of Chamberlain, Segrè, and Wiegand¹ at this energy, and is complementary to the recent work of Garrison⁹ and of Fischer and Goldhaber.¹⁰

Several authors^{1, 28, 29} have pointed out the existence of a set of

inequalities which form a necessary restriction on the behavior of the neutron-proton and proton-proton scattering cross sections, if the law of charge-independence of nuclear reactions is to be obeyed. These are quite general, and make no assumptions as to the specific nature of the potential assumed. They hold equally well for interactions not describable by a potential.

In view of the general applicability of these inequalities, and the fact that some of the recent high-energy proton-proton data³⁻⁵ have appeared to satisfy them only marginally,²⁹ it was felt desirable to measure the proton-proton scattering cross section by an independent method. The existing differential scattering data might then be accurately normalized and checked. The failure of the hypothesis of charge-independent nuclear forces would be important physical information. Chapter III describes a measurement of total proton-proton scattering at three energies, made by observing the attenuation occurring in a liquid-hydrogen target.

II. SMALL-ANGLE EXPERIMENT

A. Experimental Design

1. General

The chief problem encountered in high-energy proton-proton scattering at small angles is the high background. There are two sources of this high background: (a) scattering from the material through which the beam must pass to enter and leave the target, and (b) scattering from the edges of the collimator that serves to establish the size and direction of the incident beam. Background from the former source is primarily elastic diffraction scattering from the wall materials of the target, if liquid, or other elements in the compound if a hydrogenous compound is used. There is no way of distinguishing between the diffraction scattering and the desired hydrogen scattering, since both take approximately the same route to the detector and have the same energy at these small angles (the additional detection of the proton partners in the p-p case is not possible because of their vanishing energy). Therefore, the relative hydrogen content of the target must be kept as high as possible. With diffraction cross sections of about 10^{-24} cm²/steradian for carbon at small angles, and proton-proton (laboratory system) cross sections in the neighborhood of 2×10^{-26} cm²/steradian, the problem is not minor. The hydrogenous compound is seen to be ruled out immediately in favor of the liquid. The thickness of liquid hydrogen has an upper limit set by the multiple scattering, energy degradation, and deterioration of angular resolution permitted. Thus we see that the maximum permissible wall thickness is fairly well determined (say, by assuming hydrogen effect equal to background at worst angle). It turns out that in this experiment it is just possible to meet the safety and insulation requirements of liquid hydrogen and still stay within this upper limit on the wall thickness. A description of the target actually used appears in a later section.

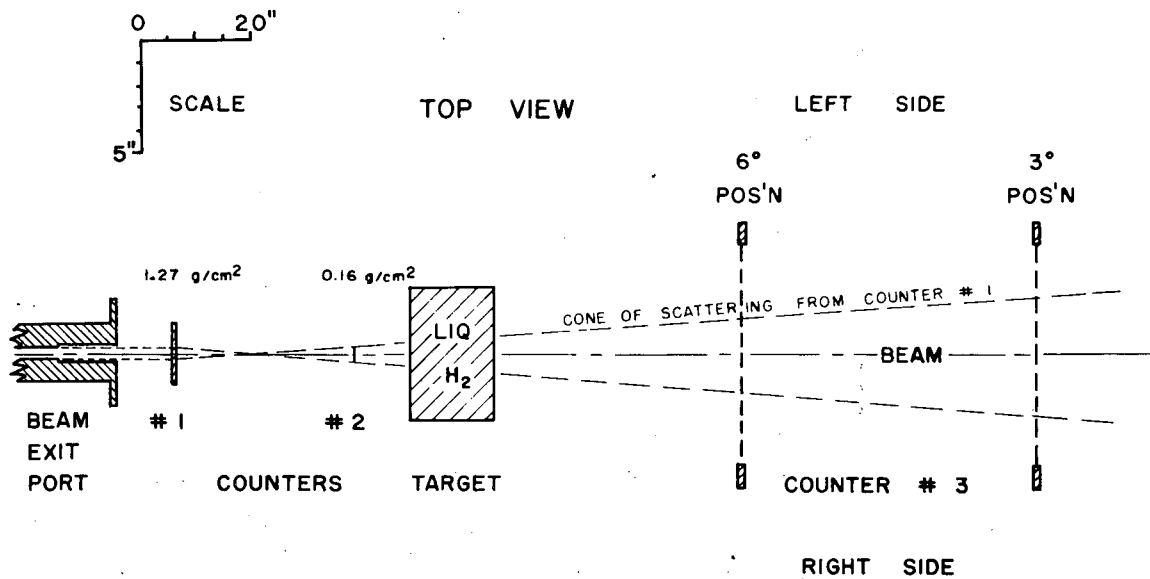
The problem of avoiding prohibitive amounts of collimator spray background (beam particles scattered by the collimator material) may be attacked from either of two rather different directions. It may be possible to deflect, precollimate, and analyze the internal beam of the

cyclotron in such a way that it passes cleanly through the final collimator into the experimental area without scraping the collimator sides. In order to obtain satisfactory results, this method requires that the circulating beam be deflected by a process that preserves the homogeneity of the beam energy. Electrostatic deflection meets this requirement but scattering from an internal target does not. In particular, the polarized beam obtained by scattering from an internal target in the 184-inch Berkeley synchrocyclotron has a broad distribution in energy and emergent angle as it reaches the last (48-inch) collimator. Since we wished to do a small-angle scattering experiment using the polarized beam, in order to obtain simultaneously the polarization and cross section, some other means of reducing the effects of collimator spray had to be sought.

Another method of reducing the background encountered from collimator spray at small angles consists of requiring a coincidence between two counters placed in the path of the beam just before it strikes the target. Such a system of electronically defining an allowed trajectory was employed in this experiment. Figure 1 displays the geometrical features of the method. It is clear that scattering from counter No. 2 adds to the background discussed under (a) of this section, and that this counter must therefore be kept as thin as possible, even at the sacrifice of some counting efficiency.

This collimation method, although reducing background, places a rather severe restriction on the counting rate. Because the beam incident on the scattering target is being counted with the scattered protons in coincidence, the limitations imposed by the finite resolution time of the coincidence and scaling systems, together with the beam time structure of the cyclotron, determine a maximum allowable flux of particles. This is shown in a later section to be on the order of 1000 protons per second.

If the scattering data are to be collected in a reasonable length of time without exceeding the restrictions on the incident beam, the solid angle viewed by counter No. 3 must be as large as possible. For best angular resolution at a given solid angle, the counter must take the shape of an annulus centered on the beam. Because the construction of such a counter is a moderately complicated undertaking, the same counter is



MU-8540

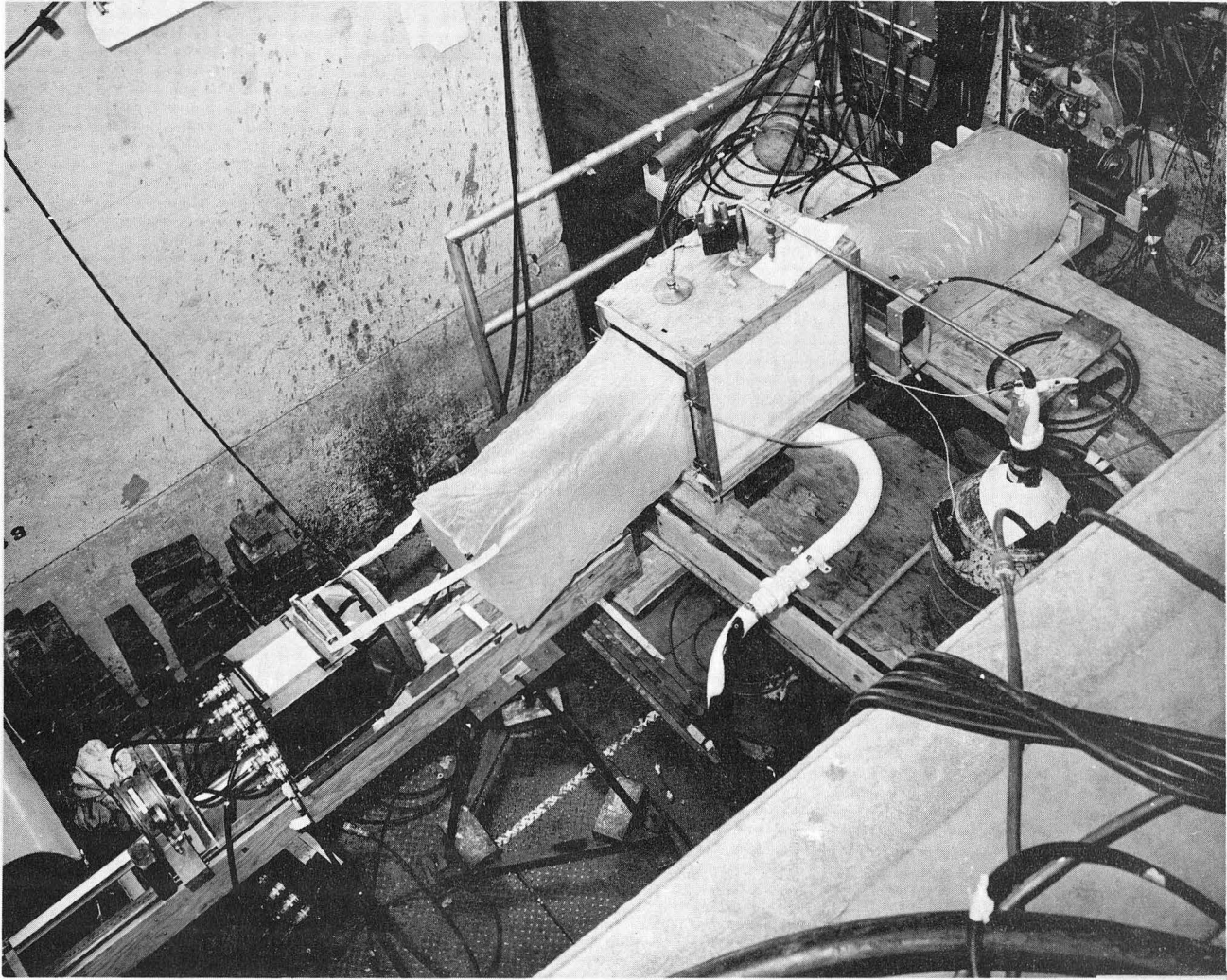
Fig. 1. Schematic geometry of small-angle experiment. Note lateral expansion of scale.

used for taking data at all the desired angles of scattering by changing the distance between it and the target. Two such positions are shown in Fig. 1. A photograph of the over-all experimental setup during a run is shown in Fig. 2.

2. Target

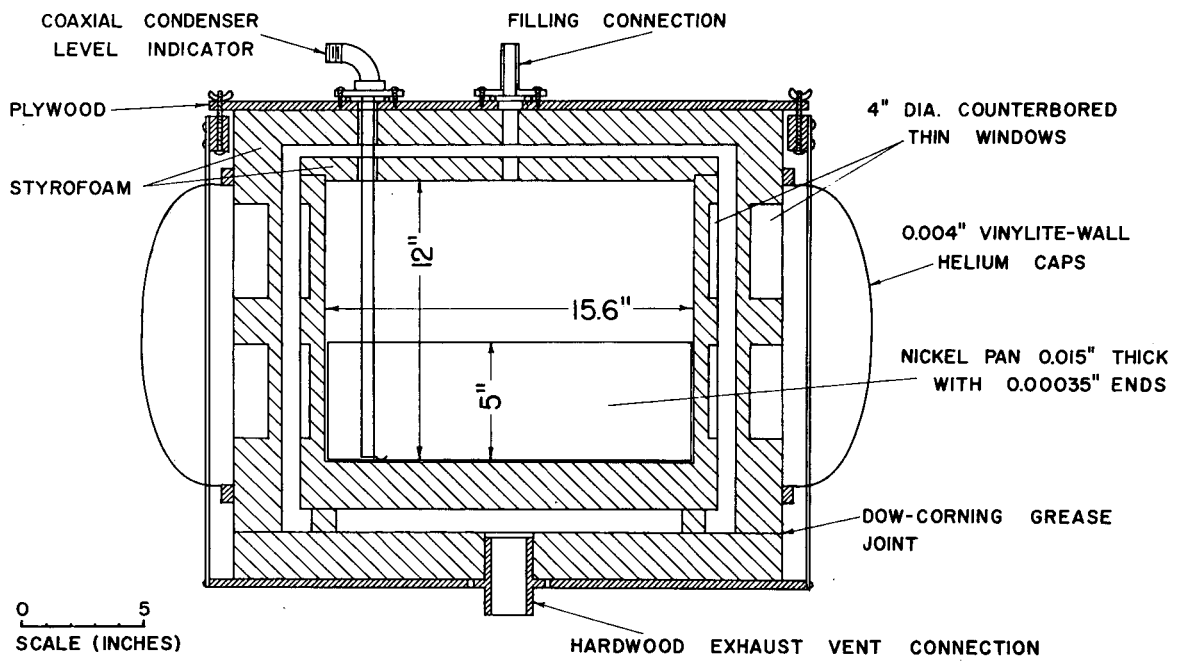
The target chosen for this experiment is of a type used first at Chicago. Polystyrene foam (trade name styrofoam) provides both container and insulation for the liquid hydrogen. Although the rate of loss of liquid hydrogen is substantially greater in this type of target than in a vacuum-jacketed metal target, the cost and complexity are significantly less. The wall-to-hydrogen ratio (in grams per square centimeter) may be made somewhat smaller for this type of target, and since the wall is of lower-Z material, the diffraction scattering from it is much less. During the early stages of this series of experiments, an attempt was made to construct a metal target of suitable size. The severe contraction under cooling when the hydrogen was introduced, however, caused repeated failures. All in all, the adoption of the styrofoam target was felt to be a happy solution to many of the target problems.

A cross-sectional diagram of the target used appears in Fig. 3, with the important dimensions indicated. The total window thickness through which the beam passes in traversing the target is 2.5 inches or 0.22 g/cm^2 of styrofoam. Above the windows viewing the liquid hydrogen is a duplicate set, which can be brought into alignment with the beam by lowering the target 6 inches. By maintaining the liquid hydrogen level well below the upper set of windows but sufficiently above the lower to ensure hydrogen in the lower path at all times, we were able to take frequent interspaced measurements of background and background plus effect. Thus effects due to slow variations in ambient background and possible slight shifts in counting efficiencies were minimized. The position of the target wherein the beam passes through the upper set of windows is called the "blank" position; the position that sends the beam through the lower windows is called the "hydrogen" or "empty" position depending on whether the target contains liquid hydrogen or not. Careful measurements of the ratio of "empty" to "blank" before filling the



ZN-1056

Fig. 2. Photograph of small-angle experimental setup.



MU-8541

Fig. 3. Cross section of thin-walled styro-foam liquid-hydrogen target.

target indicate that the blank position fulfills its role to within a few per cent.

The level of liquid hydrogen in the target is measured by the change in capacitance of a coaxial condenser immersed in the liquid to one side of the beam path. This condenser determines the frequency of an associated radiofrequency oscillator whose output is led back to the data-taking position and allows a continuous monitoring of the target condition. Dr. Clyde Wiegand of this laboratory has constructed and tested this liquid-level indicator, and has succeeded in making it an extremely reliable and sensitive device.

The bottom 5 inches of the inner styrofoam box is fitted with a nickel liner insert. This nickel liner has 0.0004-inch windows through which the beam passes, but sufficiently thick sides (0.015 inch) to maintain its rigidity. The end windows are too thin to produce any appreciable scattering of the beam. Since the liquid hydrogen level is maintained at approximately 6 inches, this liner is normally overfilled and acts to deflect bubbles generated by boiling of the hydrogen at the bottom and sides of the inner styrofoam box and to keep them out of the region seen by the beam. It is also felt that this liner furnishes a degree of safety in the event that the inner styrofoam box should rupture. Fortunately, this second feature has never been put to a test. It is interesting to note that during filling and evaporation of the liquid hydrogen in the target the point where the liquid level reaches the nickel liner top was apparent as a brief pause in the change of level. This ensures that the liner has no significant leaks and also provides an additional calibration of the level indicator.

The helium-filled end caps are necessary to prevent the formation of ice by condensation of moisture on the thin styrofoam windows.

3. Geometry and Counters

The scattering geometry is shown schematically in Fig. 1. The lateral scale has been expanded by a factor of four to show more clearly the angles defined by the various counters.

The polarized beam used in this experiment is obtained by scattering the internal proton beam of the 184-inch Berkeley cyclotron from a 1-inch-thick beryllium target. As demonstrated in previous experi-

ments,^{23, 30} this beam is highly polarized. The scattered beam is analyzed and brought out by the fringing field of the main cyclotron magnet, through a first collimating slit, a further bending magnet, and then into a 48-inch-long collimator through concrete shielding into the experimental area. Range and second-scattering experiments²⁶ show that this beam has an energy of approximately 310 Mev and a polarization of 0.74 ± 0.02 . This last collimator is a brass insert whose inside diameter is 0.5 inch for the first 38 inches of length and then widens out to 0.75 inch for the last 10 inches. This opening of the exit end provides some shielding of collimator scattering at larger angles, but offers essentially no assistance at the small angles considered in this experiment. Its use here is a matter of convenience only.

The first counter is placed as close to the exit end of this collimator as is possible, and the second as close to the target as possible, in order to keep the lever arm of their collimation as long as possible. The length of the experimental area is limited by heavy shielding blocks at the rear, and there is a premium on using it efficiently.

Counter No. 1 is a box of thin lucite 3 by 3 inches square by 0.5 inch (1.27 g/cm^2) thick, containing terphenyl dissolved in phenylcyclohexane as a liquid scintillator. This active volume is viewed through a lucite light pipe by a type 5819 RCA photomultiplier tube. The optical efficiency is quite good; direct measurements show that for protons of this energy the pulse-height resolution is a distribution roughly 20 percent wide at half maximum (see Fig. 16).

Counter No. 2 is a disc of plastic scintillator 0.75 inch in diameter by $1/16$ inch (0.159 g/cm^2) thick, viewed edgewise by two type 5819 photomultipliers connected in parallel. The shadow of this counter in the beam scattered from the collimator or first counter is shown by dotted lines in Fig. 1. It will be seen that in order to pass through counters Nos. 1, 2, and 3 a particle must be scattered either from counter No. 2 or from the target. The edges of this shadow, of course, are blurred by multiple scattering in the liquid hydrogen; for the 2.80 g/cm^2 of hydrogen in the target, the rms angle of deviation is 0.5° . At the minimum laboratory-system scattering angle of 3° , counter No. 3 is still well protected from any undesired particles.

Counter No. 3 is a split annular-type counter, divided into two parts along a vertical diameter as shown in Fig. 4. It is designed to be rotated about an axis parallel to the incident beam in order to verify that the response of the two counter halves is equal. Each half of the counter is viewed by 3 type 5819 photomultipliers connected in parallel. It is furnished with a set of iron ring absorbers variable in steps of 5 g/cm^2 out to 100 g/cm^2 . As shown by the derivation in Appendix C, it is desirable to place counter No. 3 as far as possible from the target in order to minimize the effect of finite target size on the angular resolution.

The limited extent of the experimental area prevents a complete optimizing of the scattering geometry in this experiment. Referring to Fig. 5, it may be seen that increasing the distance \underline{d} from the center of the target to the rear counter No. 3 (and, of course, increasing the counter radius \underline{a} to maintain the same angle of measurement) would not greatly improve the angular resolution at the smallest angles, since this is set by multiple scattering in the target and the necessary solid angle subtended by the rear counter. At the larger angles obtained by decreasing the distance \underline{d} and maintaining the counter radius \underline{a} , however, the resolution is seriously degraded by the finite extent of the target. Unfortunately, this is the consequence of limited space and this type of counter design.

One other piece of equipment deserves mention here. A method is needed to change the angle of measurement and at the same time maintain accurate alignment of counter No. 3 with respect to counters Nos. 1 and 2 and with the beam. It was finally decided that a track resembling closely an optical bench provided the most satisfactory solution. This track is aligned photographically with the beam as described in a later section and allows counter No. 3 to be moved precisely and reproducibly.

4. Electronics

The electronics for this experiment were centered around a fast multiple-input coincidence unit³¹ and a fast scaling circuit.³² Both of these were adapted and constructed by Dr. Clyde Wiegand of this laboratory. It should be emphasized that it was the development of the scaling circuit with 10^{-8} -second resolution that made this experiment feasible.

A block diagram of the electronic system is shown in Fig. 6. The

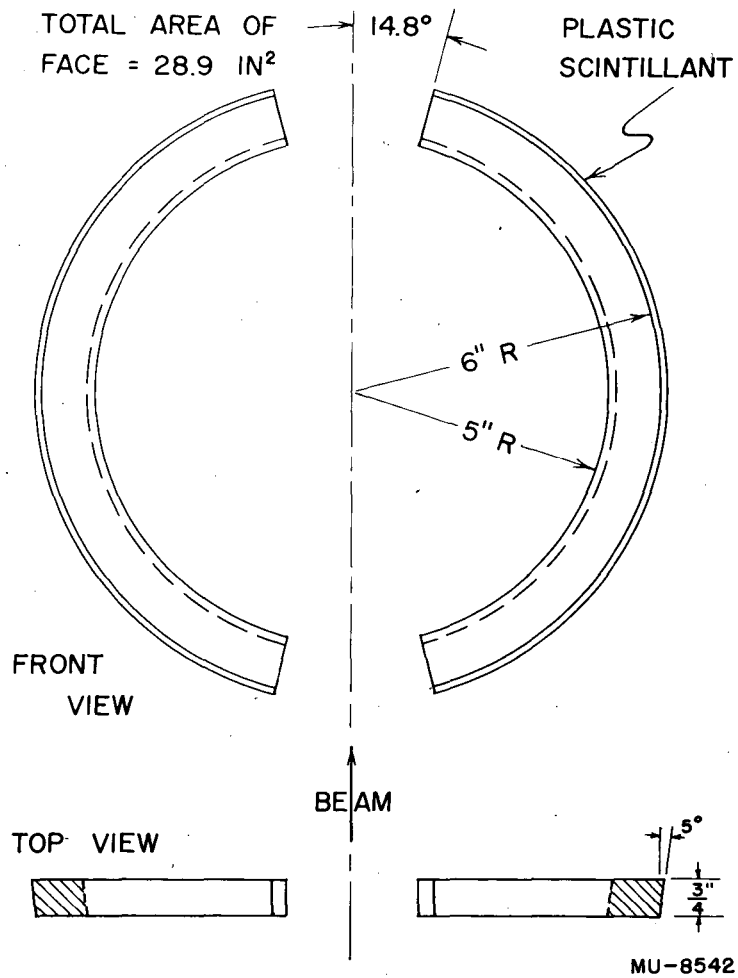
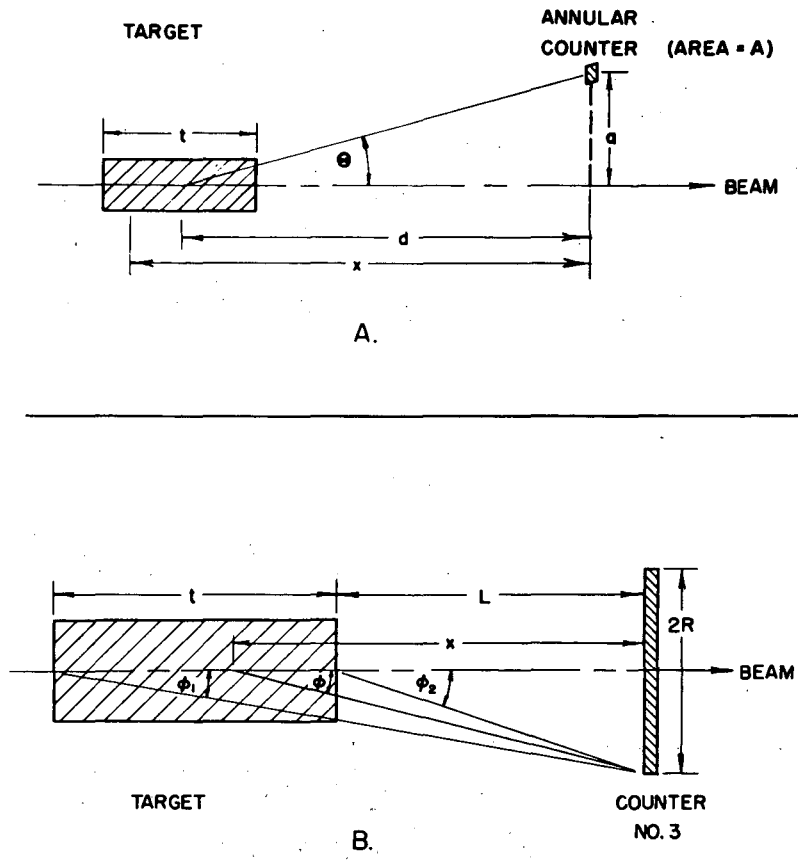


Fig. 4. Diagram of the active portion of the annular counter No. 3, showing its dimensions and position with respect to the beam.



MU-8543

Fig. 5. Target and rear counter geometries, (A) small angle, (B) attenuation.

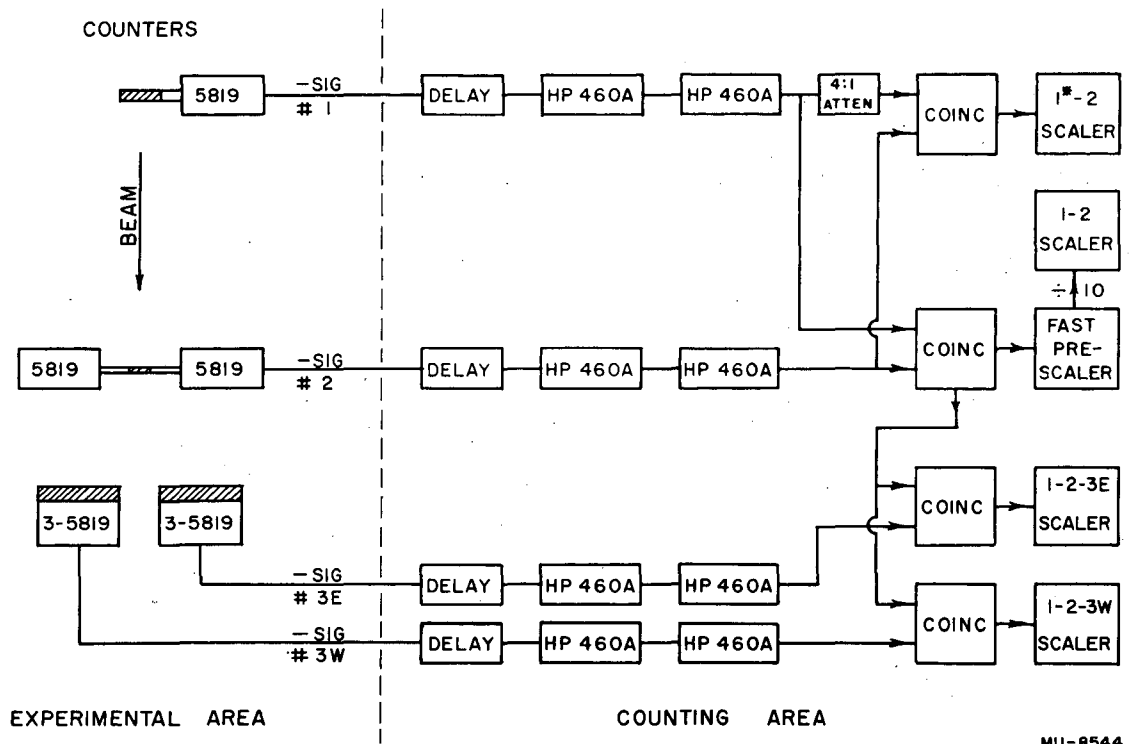


Fig. 6. Block diagram of electronics for small-angle experiment.

high-voltage connections to the photomultipliers are not shown. The operation of the system is as follows: a proton passes through counters Nos. 1 and 2 and registers a coincidence count on the fast scaler. If this particle scatters into either the "east" or "west" sides of the annular counter, then there is in addition a count from the corresponding side of the next coincidence circuit.

The method of producing the polarized beam leads to a fine structure with respect to time of the probability of receiving beam protons. The internal beam of the cyclotron occupies about 30° of the phase of the 16.7 mc/sec radiofrequency accelerating voltage. For a moderate time after the internal beam has been accelerated out to the maximum usable radius, the internal target strips off a fraction of the particles and sends them on to the experimental area. Therefore, the time structure of the beam consists of 60 course-structure bursts per second (the repetition rate of acceleration cycles), each of which contains roughly 200 fine-structure bursts 0.5×10^{-8} second wide and spaced 6.0×10^{-8} second apart.³³

As the resolving time of the electronic circuits used in the present experiment is about 2×10^{-8} second, it may be said that there are about 12,000 fine-structure bursts each second. It is seen that this is equivalent to sorting all beam particles into very short time intervals (of which there are 12,000 per second). Any two counter pulses occurring within one of these fine-structure bursts appear to the counting equipment as simultaneous.

There are at least two varieties of error that are introduced by failure of the system to resolve. If two legitimate beam particles arrive during the same fine-structure burst, the monitoring system sees them as one, but the probability that at least one of them scatters is doubled. Thus, the apparent cross section is raised. Or there may be a collimator-scattered particle traveling directly to the annular counter accompanied by a legitimate particle traversing counters Nos. 1 and 2, which opens the gate and allows the undesired particle to be counted as a scattering event. Events of this kind appear as an increase in the background.

The probabilities of occurrence of these effects are worked out in

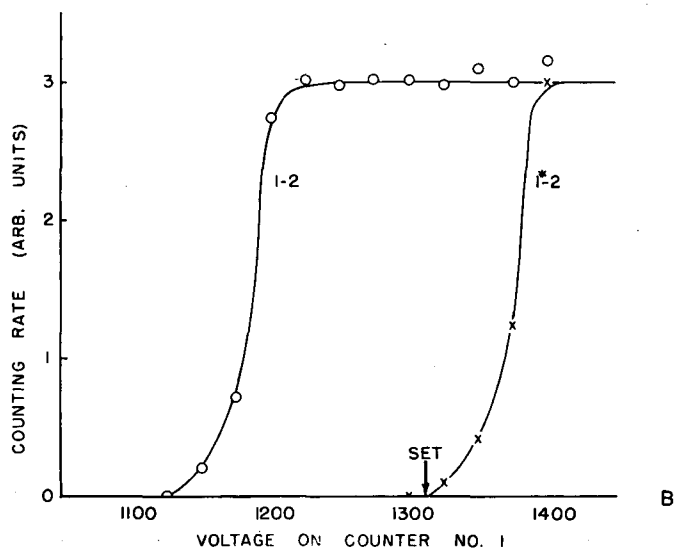
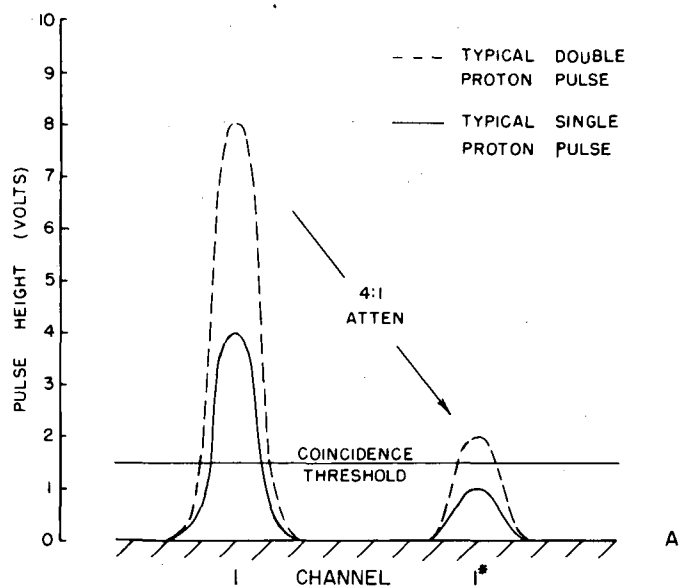
Appendix A. In our case, the τ appearing in the Poisson law is an effective resolving time, including effects of the machine's duty cycle and the finite resolving time of the counter-coincidence system. Conceptually, it is probably easier to visualize the reciprocal, $1/\tau$, which is the number of effective resolving times occurring per second. From the preceding discussion it is clear that $1/\tau$ is equal to the effective number of fine-structure bursts per second, for our system. Thus, if $N\tau \ll 1$, $N\tau/2$ is the fraction of double pulses occurring, and $N\tau$ is the factor by which collimator spray is suppressed.

If the pulse received from counter No. 1 is longer than the width of a fine-structure burst, then two or more protons passing through the pulse-height counter No. 1 in the same window give an output pulse at least twice as great as normal. Therefore, the output from counter No. 1 is split off, run through a 4:1 attenuator, and placed in coincidence with counter No. 2. This attenuated channel is called 1^* and the coincidence rate 1^*-2 is a direct measure of multiple pile-up.

Figure 7 shows the relative pulse heights in Channels 1 and 1^* , for a single- and for a double-proton pulse. The procedure followed to set the pulses to these levels is described in a later section. Fluctuations in the coincidence threshold for the 1^* channel due to varying pulse heights in the No. 2 channel were minimized by running the No. 2 counter far up on its plateau, i. e. by making certain that every No. 2 pulse completely cut off the corresponding input coincidence tube. Figure 7 indicates that the full width at half maximum of the pulse-height distribution of counter No. 1 should be significantly better than 50 percent if separation is to be reliably achieved. The observed value of approximately 20 percent (see Fig. 16) is felt to be adequate.

The possibility of using the 1^*-2 coincidences in anticoincidence with both 1-2 and 1-2-3 events (and thus eliminating the effects of collimator spray and high 1-2 counting rates) was considered, but was prevented by existing equipment limitations.

The correction necessitated by pile-up in the 1-2 channel was made by dividing the final values of cross section by the factor $1 + \frac{n(1^*-2)}{n(1-2)}$, where $n(x-y)$ is the x-y coincidence counting rate. Because the cross section data were all taken at the same 1-2 counting rate, the relative



MU-8545

Fig. 7. A) Single- and double-pulse conditions in channels 1 and 1*. B) Plateau of counter No. 1 seen in both channels.

values were unaffected. The collimator spray contribution, of course, was removed in the background subtraction.

B. Procedure

1. Line-up

Line-up was accomplished by exposing film at four points along the beam path in the experimental area. X-ray-type film was placed adjacent to counters No. 1 and No. 2, and at the two extreme positions on the bench supporting counter No. 3. The film holders were designed to puncture the film in a way that allowed the processed film to be reproducibly replaced. By sighting through holes punched in the center of the beam pattern in these films, counters Nos. 1 and 2 and the target were placed successively in alignment with the beam.

The defining counter (No. 2) required the most critical alignment, since it partially determined the effective beam center line and therefore the scattering angle. It is estimated that this alignment was made to within $\pm 1/32$ inch. The placement of counter No. 1 was not critical as long as it covered the 0.75-inch diameter exit hole of the collimator. The same was true of the target's 4-inch windows with respect to counter No. 2. The bench supporting counter No. 3 was brought into line with the beam by the aid of two jigs with crosshairs set to mark the center of counter No. 3 when in position on the bench. The chief difficulty in this alignment was due to the spreading of the beam by multiple scattering along the air path. The error assigned here is $\pm 1/8$ inch at the forward end (10° position) and $\pm 1/4$ inch at the rear (3° position) of the counter bench.

2. Delays and Plateaus

To speed up the adjustment of the electronics, a 3.20 g/cm^2 carbon target was placed in the beam following counter No. 2. The diffraction scattering at small angles from this target provided a copious source of elastically scattered protons to facilitate bringing counter No. 3 into proper coincidence.

With the voltages on the photomultipliers set to reasonable (previously determined) values, the 1-2 coincidence rate was measured as a

function of relative delay of the signal from counter No. 1 with respect to that from counter No. 2. The singles count from counter No. 1 was used to monitor the beam. Similarly the two halves of counter No. 3 were each brought into coincidence with counters No. 1 and No. 2. Following this, curves of coincidence counting rates versus photomultiplier voltage were taken, in order to ensure that all desired pulses from the counters were being accepted. From these plots suitable operating points were selected.

Figure 7 shows the relative pulse conditions in Channels 1 and 1*, together with the response in both channels due to varying the photomultiplier voltage on counter No. 1. The data shown here were taken with such a weak beam that the 1*-2 counts due to pile-up could be neglected. The voltage was set as shown by the arrow, as far up on the plateau of No. 1 as possible but before the toe of No. 1*.

The comparatively broad pulses (2×10^{-8} second) used here allowed the photomultiplier voltages to be changed over large ranges without upsetting the delay conditions. At any rate, quick checks of the delays were always made after selecting the operating voltages.

3. Range Curves and Alignment Checks

After the electronics were set up, a range curve was taken of the protons scattered from the carbon target previously described. This curve, shown in Fig. 8, provided a further check that we were observing the desired particles. Extrapolating back through the target and counters, one can see that the range of the incident beam was approximately equivalent to 80 g/cm^2 of copper. This corresponds to an incident energy of about 310 Mev,³⁴ and is in good agreement with previous measurements³⁰ under the same operating conditions. The data used in the final determination of cross section and polarization were all taken with 1.5 inches (30 g/cm^2) of iron absorber in front of counter No. 3. This requirement on the energy of the scattered particles further prevented undesired particles from being counted.

By rotating counter No. 3 through 90° around the beam axis, one can measure differences in counting rate produced by scattering up or down in a vertical plane (at right angles to the original scattering plane which produced the polarization), and check vertical alignment of the

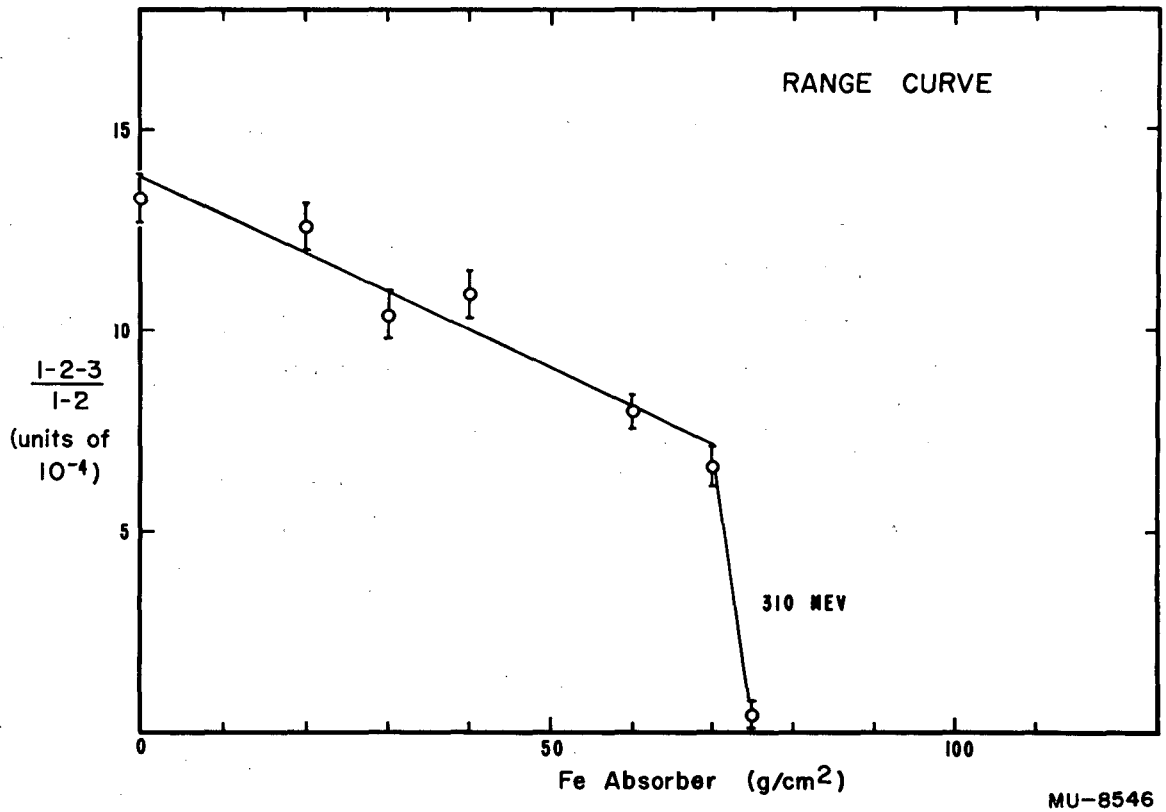


Fig. 8. Range curve for annular counter in small-angle experiment.

system. That there be no scattering asymmetry in this plane is a basic requirement of invariance of the system to reflections in space and time.³⁵ If a carbon target is used for which the differential scattering cross section is known to change rapidly with angle in this angular region, then we have a sensitive measure of how well the apparatus is aligned with the beam in the vertical dimension. Turning the counter 90° in the other direction from the normal position then interchanges the two counter halves up and down, and provides an independent check on the equivalence of response of the two halves of counter No. 3.

This method does not, of course, ensure alignment in the horizontal plane, but by measuring the degree of vertical alignment it provides reassurance that the horizontal alignment procedures are adequate.

4. Taking Data

After the alignment, plateaus, delays, and range curves had been taken, a routine of data taking was set up and followed. The individual data runs were kept as short as practicable, consistent with reading and recording the data from the scalers, in order to check reproducibility of the data and to detect gross malperformance of the equipment as early as possible. A data cycle consisted of a run with the target raised (the "hydrogen" position) and with 1.5 inches of iron absorber in front of counter No. 3, followed by two shorter runs with the target lowered (the "blank" position), using 1.5 and 2.5 inches of iron absorber. The time was divided between hydrogen and blank as the square root of the ratio of counting rates, in order to minimize the statistical error in the result. The two sets of blank data provided a continuous check on the region of interest in the range curve. Any significant increase in the number of lower-energy beam protons (due to slight changes in the cyclotron operation, for instance) would be apparent as a decrease in the ratio of counting rate at 2.5 inches of absorber to that at 1.5 inches.

In order to compensate for the effect on the proton range of the 2.80 g/cm² of hydrogen, which is not present while taking the blank data, 8.3 g/cm² of iron absorber should be added in front of counter No. 3. Averaging the blank data obtained with 1.5 and 2.5 inches of absorber is thus nearly equivalent to making this correction (the range curve in Fig. 8 is seen to be linear in this region of absorber).

The two different effects of nuclear attenuation (by scattering) and finite range in absorber should be carefully distinguished here. Inserting an amount of iron equivalent in stopping power to the liquid hydrogen in the target ensures that the scattered particles counted in the cases of hydrogen and blank data represent the same energy fraction of the incident beam. Although there was no evidence that the beam was not substantially monoenergetic, this precaution was felt to be desirable. The corrections stemming from nuclear attenuation in the target and various absorbers are discussed in the next section.

At each setting of the scattering angle, the data-taking was cycled several times through the sequence described above. In addition, a small amount of the data was taken at varying beam levels to check the dependence of the 1-2 counting rate. The angular settings chosen were dictated by the angular resolutions of the system. (see Appendix C)

C. Data Reduction and Errors

1. Cross Section Calculations

Let f be the fraction of particles traversing counters No. 1 and 2 that are also scattered into either half of counter No. 3. Let the subscript "H" denote data taken in the "hydrogen" position. The subscript "B" refers to the data taken in the "blank" position averaged over the two absorber values used. Then the fraction that is due to scattering from the hydrogen in the target is

$$\Delta H = (f_H - 1.03 f_B),$$

where a correction 1.03 has been applied to the blank data to compensate for the additional nuclear attenuation suffered. This relative attenuation of the blank data is equal to the attenuation in the additional 0.5-inch (average) iron blank-position absorber used minus that occurring in the hydrogen when in the hydrogen position. The attenuation in the iron has been estimated from the range curve of Fig. 8 as 7 percent, agreeing with Kirschbaum.³⁶ The hydrogen attenuation was directly measured as 4 percent, as reported in Chapter III.

ΔH is related to the differential cross section for scattering per hydrogen atom, $\left(\frac{d\sigma}{d\Omega}\right)_{\text{lab}}$, by

$$\Delta H = \left(\frac{d\sigma}{d\Omega}\right)_{\text{lab}} \frac{\rho}{M} \int_{\text{target}} \Omega(x) dx$$

where ρ/M is the atomic density of liquid hydrogen and the integral sums the solid angle seen by counter No. 3 for each element of the target.

Combining these factors and solving for $\left(\frac{d\sigma}{d\Omega}\right)_{\text{lab}}$, we have

$$\left(\frac{d\sigma}{d\Omega}\right)_{\text{lab}} = \eta \Delta H,$$

where η is worked out in Appendix B. The center-of-mass scattering cross section is given relativistically by

$$\left(\frac{d\sigma}{d\omega}\right)_{\text{c. m.}} = \left(\frac{d\sigma}{d\Omega}\right)_{\text{lab}} \frac{d\Omega}{d\omega},$$

where

$$\frac{d\Omega}{d\omega} = \frac{[1 + (T/2) \sin^2 \textcircled{H}]^2}{1 + T/2} \left(\frac{1}{4 \cos \textcircled{H}}\right)$$

T , the kinetic energy in the laboratory system, is measured in units of Mc^2 , and \textcircled{H} is the angle of scattering in the laboratory coordinate system. The center-of-mass scattering angle, θ , is related to the laboratory angle by

$$\tan \frac{\theta}{2} = [1 + T/2]^{1/2} \tan \textcircled{H}.$$

Table I lists the values of these quantities obtained, uncorrected for attenuation in the absorbers. The errors shown are statistical only.

Table I

| θ lab degrees | f_H units of 10^{-4} | $1.03 f_B$ units of 10^{-4} | ΔH units of 10^{-4} | η $10^4 \frac{\text{mb}}{\text{ster}}$ | $\frac{d\Omega}{d\omega}$ | uncorrected $\left(\frac{d\sigma}{d\omega}\right)$ c. m. mb/ster | θ c. m. degrees |
|-------------------------|--------------------------------|-------------------------------------|-------------------------------------|--|---------------------------|--|---------------------------|
| 3.0 | 4.13 ± 0.09 | 2.19 ± 0.08 | 1.95 ± 0.12 | 22.60 | 0.2130 | 9.38 ± 0.59 | 6.5 |
| 3.5 | 3.80 ± 0.11 | 1.95 ± 0.07 | 1.85 ± 0.13 | 16.58 | 0.2133 | 6.54 ± 0.46 | 7.6 |
| 4.0 | 3.47 ± 0.08 | 1.90 ± 0.07 | 1.56 ± 0.11 | 12.76 | 0.2135 | 4.25 ± 0.29 | 8.7 |
| 5.0 | 3.77 ± 0.09 | 1.53 ± 0.07 | 2.24 ± 0.12 | 8.083 | 0.2140 | 3.88 ± 0.20 | 11.0 |
| 6.0 | 4.50 ± 0.08 | 1.49 ± 0.07 | 3.02 ± 0.11 | 5.589 | 0.2145 | 3.62 ± 0.13 | 13.0 |
| 8.0 | 6.89 ± 0.09 | 1.87 ± 0.06 | 5.02 ± 0.11 | 3.133 | 0.2160 | 3.40 ± 0.07 | 17.3 |
| 10.0 | 9.42 ± 0.14 | 1.76 ± 0.09 | 7.66 ± 0.16 | 1.967 | 0.2180 | 3.29 ± 0.07 | 21.7 |

a. Corrections. The major correction is necessitated by attenuation of the scattered particles in the 30 g/cm^2 iron absorber in front of counter No. 3. This correction is estimated from the range curve of Fig. 8 or from Kirschbaum's data³⁶ to be 1.22.

The attenuation of particles (either primary beam or scattered) in passing through the hydrogen in the target is described in Chapter III to be 0.04, leading to a correction of 1.04.

The fractional pile-up in the 1-2 channel is $\frac{n(1^*-2)}{n(1-2)} = \frac{N\tau}{2}$, as shown in Appendix A. In our experiment, at a 1-2 counting rate of 800 per second, this was measured to be 0.03 (see Section A4), leading to a correction of about 0.97 in the cross section.

The cold hydrogen gas seen in the blank position leads to a correction of 1.02. This is discussed more fully at the end of Chapter III.

Since the proton beam loses 22 Mev³⁴ in traversing the liquid hydrogen in the target, the mean energy of scattering has been taken as 300 Mev.

Table II lists the corrections applied and the final absolute values obtained. Column 5 contains the final values normalized to a value of 3.75 mb/ster at 21° center-of-mass. Figure 9 is a plot of these normalized values versus the center-of-mass scattering angle. The fact that this normalization changes only slightly the absolute values obtained leads to an increased confidence in the methods employed. It is felt, however, that the relative values of differential cross section are probably subject to less error than the absolute values, and we are thus justified in normalizing to the more accurate value at large angles obtained in Chapter III.

The angle of scattering shown in each case is that between the beam direction and a line drawn from the center of the target to the mean radius of counter No. 3. The resulting angular resolutions are worked out in Appendix C, and itemized in Table VIII. Column 6 in Table II gives twice the total rms center-of-mass angular deviation as a measure of angular resolution for each mean angle of scattering.

b. Errors. The errors in the values of cross section quoted arise from three sources: (a) counting statistics, (b) systematic error in the determination of the distance between the target and counter No. 3,

Table II

| θ c. m. degrees | uncorrected $\left(\frac{d\sigma}{d\omega}\right)$ c. m. mb/ster | corr. factor | corrected $\left(\frac{d\sigma}{d\omega}\right)$ c. m. mb/ster | normalized $\left(\frac{d\sigma}{d\omega}\right)$ c. m. mb/ster | $2\sqrt{\Sigma \delta \theta^2}$ c.m. degrees |
|------------------------------|---|-----------------|---|--|---|
| 6.5 | 9.38 ± 0.59 | 1.25 | 11.73 ± 0.74 | 10.71 ± 0.74 | 2.9 |
| 7.6 | 6.54 ± 0.46 | 1.25 | 8.17 ± 0.58 | 7.46 ± 0.58 | 3.0 |
| 8.7 | 4.25 ± 0.29 | 1.25 | 5.31 ± 0.36 | 4.85 ± 0.37 | 3.2 |
| 11.0 | 3.88 ± 0.20 | 1.25 | 4.85 ± 0.26 | 4.42 ± 0.27 | 3.5 |
| 13.0 | 3.62 ± 0.13 | 1.25 | 4.52 ± 0.18 | 4.13 ± 0.20 | 3.9 |
| 17.3 | 3.40 ± 0.07 | 1.25 | 4.25 ± 0.14 | 3.88 ± 0.17 | 5.3 |
| 21.7 | 3.29 ± 0.07 | 1.25 | 4.11 ± 0.16 | 3.75 ± 0.18 | 7.3 |

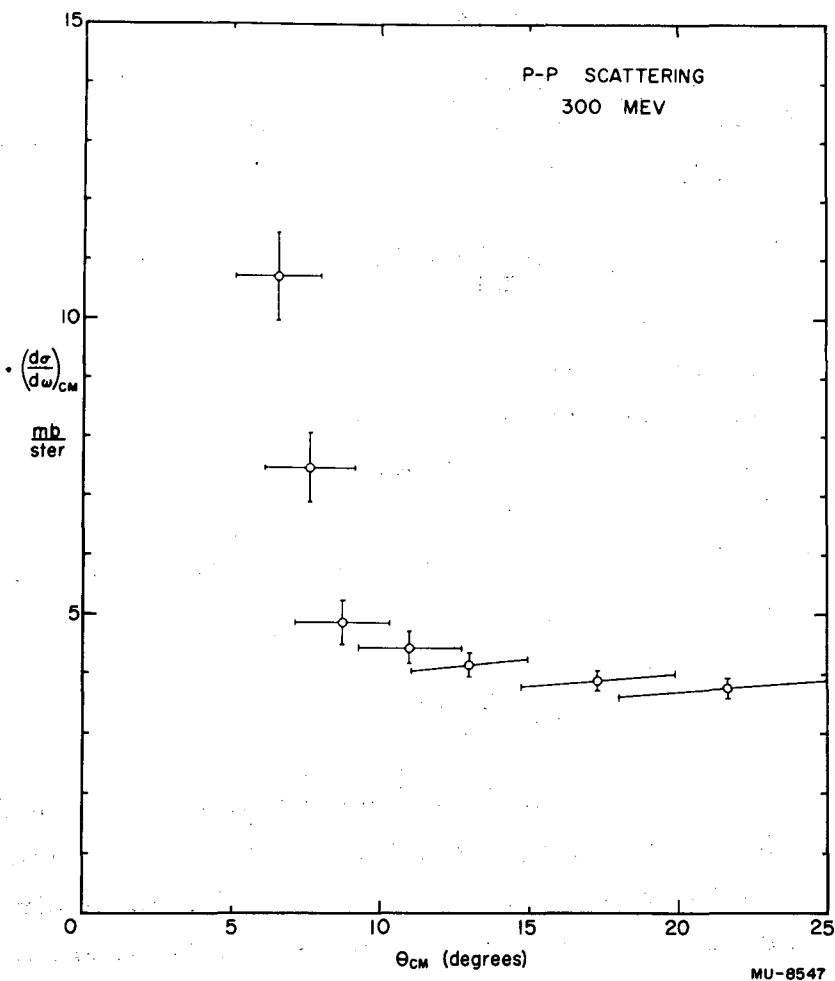


Fig. 9. Differential cross section as a function of center-of-mass scattering angle.

(c) error in the value of cross section to which the 21° data were normalized.

The standard deviation of the statistical errors are shown in Table I and Column 2 of Table II. The corrected values in Column 4 contain the estimated systematic error, corresponding to an uncertainty of 0.5 inch in the measurement of the target-counter No. 3 separation. The error from the normalization value at 21° used has been folded into the results shown in Column 5. Figure 9 includes the final errors and indicated angular resolutions.

2. Polarization Calculations

The asymmetry of scattering into the east and west halves of counter No. 3 is defined as

$$e' = \frac{(\Delta H)_E - (\Delta H)_W}{(\Delta H)_E + (\Delta H)_W},$$

where $(\Delta H)_{E, W}$ has the same meaning as in the previous section, except that the subscripts restrict the measurements to the east or west sides of counter No. 3, respectively.

It is shown in Appendix D that, owing to the finite extension of counter No. 3 over the azimuthal angle of scattering, ϕ , the true $\phi = 0, 180^\circ$ asymmetry is given by

$$e = \frac{\Delta \phi}{\sin(\Delta \phi)} e',$$

where $2\Delta\phi$ is the azimuthal angular span of either half of counter No. 3.

If the scattering is elastic, it may be shown that the asymmetry produced by the scattering of a polarized beam is simply the product of the polarization of the incident beam and the polarization that would be produced in scattering an unpolarized beam from the same target at the same polar angle θ . Thus the polarization produced by the target is given in terms of the measured quantities by

$$P(\theta) = \frac{e(\theta)}{P_{\text{inc}}} = \frac{\Delta \phi}{P_{\text{inc}} \sin(\Delta \phi)} \frac{(\Delta H)_E - (\Delta H)_W}{(\Delta H)_E + (\Delta H)_W},$$

where $\frac{\Delta \theta}{\sin(\Delta \theta)} = 1.358$ for counter No. 3. P_{inc} has been measured in a previous experiment²⁶ to be 0.74 ± 0.02 .

Table III lists the quantities that enter into the determination of P. A weighted average of the asymmetries obtained at the two counting rates has been taken for the last two columns.

a. Corrections. The same blank correction (1.03) has been used in calculating $(\Delta H)_{E, W}$ as was used in the determination of $(\Delta H)_E - (\Delta H)_W = \Delta H$. All other corrections necessary to the cross section cancel out of the expression for the asymmetry.

b. Errors. Statistical errors in the asymmetry have been calculated from the expression

$$\delta e' \cong \frac{\sqrt{2}}{4} \left[\frac{\delta(\Delta H)_E}{(\Delta H)_E} + \frac{\delta(\Delta H)_W}{(\Delta H)_W} \right],$$

which holds if $(\Delta H)_{E, W}$ are approximately equal. These errors are shown in Column 5 of Table III.

The systematic errors arising from misalignment of the counter axis with the beam become quite serious in the Rutherford scattering region where the cross sections are rapidly changing with angle. The necessary expressions are worked out in Appendix E. For an estimated error in alignment of ± 0.25 inch (see Section B1) at the rear of the counter bench, the error in asymmetry amounts to ± 0.18 . This error has been folded into Columns 6 and 7 of Table III for the two smallest angles where the cross section data show a roughly Rutherford variation. It should be mentioned that errors of this type cancel to first order in forming the cross section.

The polarization results, except for the two smallest angles where the errors make the results almost meaningless, are plotted in Fig. 10. The angular resolutions shown are those calculated in Appendix C.

Table III

| θ c.m. degrees | 1-2 ctg. rate sec ⁻¹ | $(\Delta H)_E$ units of 10 ⁻⁴ | $(\Delta H)_W$ units of 10 ⁻⁴ | e' statistical errors only | e total errors shown | P total errors shown |
|-----------------------------|---------------------------------------|--|--|------------------------------------|---------------------------|---------------------------|
| 6.5 | 800 | 0.862 ± 0.091 | 1.086 ± 0.094 | -0.115 ± 0.068 | -0.16 ± 0.20 | -0.21 ± 0.27 |
| 7.6 | 800 | 1.001 ± 0.096 | 0.847 ± 0.095 | 0.058 ± 0.073 | 0.08 ± 0.21 | 0.11 ± 0.28 |
| 8.7 | 800 | 0.788 ± 0.081 | 0.774 ± 0.077 | 0.009 ± 0.071 | 0.01 ± 0.10 | 0.02 ± 0.13 |
| 11.0 | 800 | 1.25 ± 0.09 | 0.99 ± 0.08 | 0.112 ± 0.055 | 0.14 ± 0.05 | 0.19 ± 0.07 |
| 11.0 | 2000 | 1.41 ± 0.10 | 1.18 ± 0.08 | 0.087 ± 0.052 | | |
| 13.0 | 800 | 1.72 ± 0.08 | 1.29 ± 0.08 | 0.14 ± 0.04 | 0.19 ± 0.04 | 0.25 ± 0.05 |
| 13.0 | 1500 | 1.79 ± 0.10 | 1.37 ± 0.09 | 0.13 ± 0.04 | | |
| 17.3 | 800 | 2.83 ± 0.08 | 2.19 ± 0.07 | 0.13 ± 0.02 | 0.18 ± 0.03 | 0.25 ± 0.04 |
| 17.3 | 1500 | 2.66 ± 0.16 | 1.92 ± 0.14 | 0.16 ± 0.05 | | |
| 21.7 | 800 | 4.59 ± 0.13 | 3.08 ± 0.10 | 0.20 ± 0.02 | 0.27 ± 0.03 | 0.37 ± 0.04 |

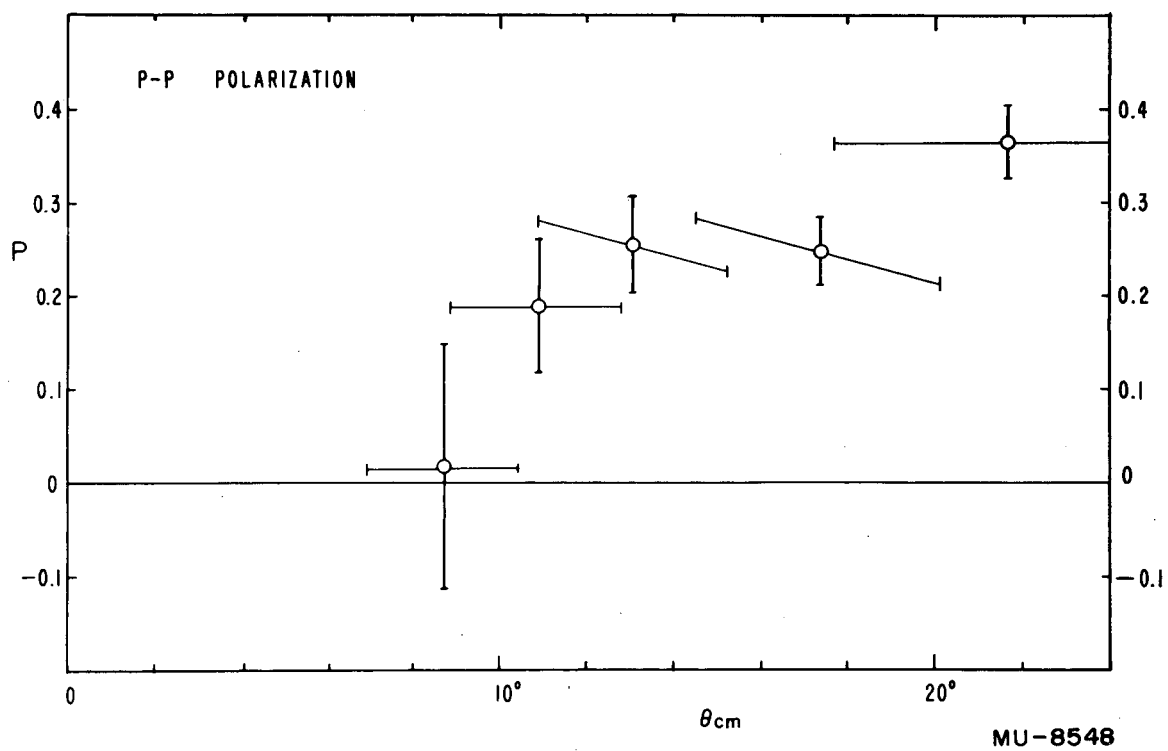


Fig. 10. Polarization as a function of center-of-mass scattering angle.

III. ATTENUATION EXPERIMENT

A. Method

1. General Description and Layout

The measurement of the total proton-proton scattering cross section by attenuation was performed using the standard unpolarized internally scattered³⁷ proton beam from the 184-inch synchrocyclotron. The general layout is shown in Fig. 11. A schematic diagram of the experimental geometry appears in Fig. 12.

Because the reliable measurement of a small attenuation depends critically on the good behavior of electronic coincidence and scaling systems, an alternative photographic method was used for a large fraction of the initial data collected, in order to gain confidence in the more conventional electronic techniques.

2. Collimation and Energy Reduction

The path of the scattered proton beam is shown in Fig. 11. Energy reduction was achieved by inserting absorber on the large cyclotron probe before the analyzing magnet, in a manner first used by Kirschbaum.³⁶ Owing to the extremely "good" geometry imposed by the long path through the analyzing magnet and 48-inch collimator, even small amounts of internal absorber result in an appreciable attenuation of the external beam. Since multiple and diffraction scattering rise rapidly with atomic number, beryllium was used when available, carbon otherwise. The range curves obtained with the internal absorbers used are shown in Fig. 15. The procedure followed in taking these range curves is described in Section B3.

Since the incident beam in the experimental area was to be monitored by counters placed in the beam before striking the target, it was felt that these counters should also act as beam collimators, in order to minimize the energy degradation resulting from scattering from the sides of a small collimator tube. Consequently, a 48-inch-long collimator, 2 inches in diameter, was used. In addition to having a larger ratio of area to circumference, this collimator permitted taking advantage of the beam pattern to reduce somewhat the intensity at the collimator walls.

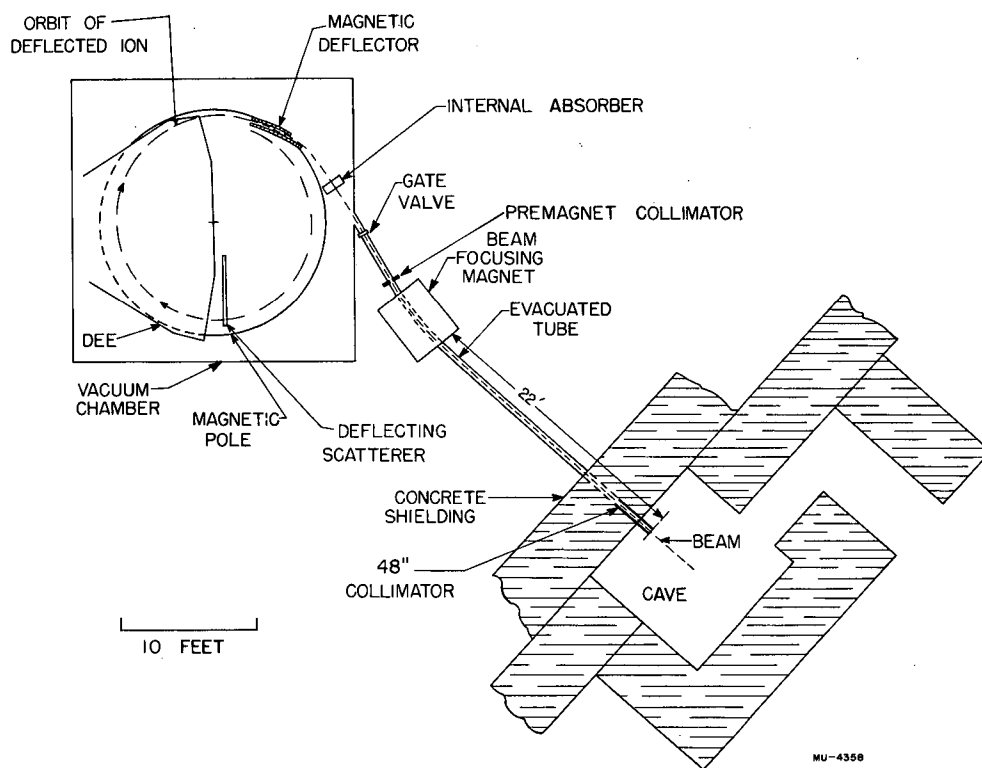


Fig. 11. Cyclotron layout showing placement of internal absorber.

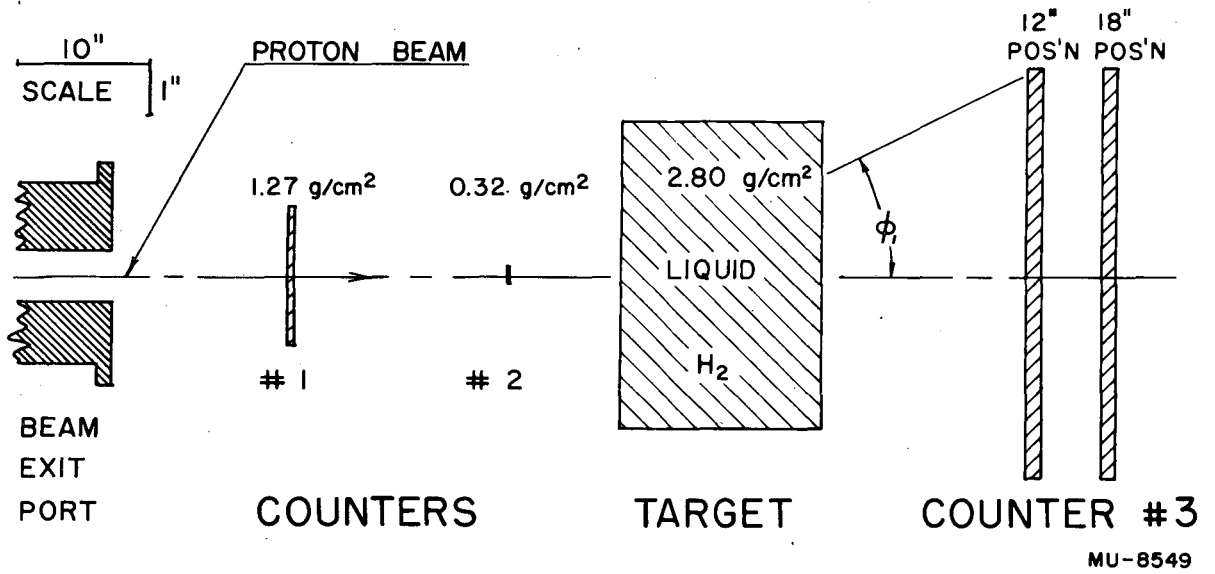


Fig. 12. Schematic geometry of attenuation experiment. Note lateral expansion of scale.

Consistent with maintaining a small beam pattern, the premagnet collimator would normally be opened as far as possible to maintain the ratio of internal circulating beam to external beam (and therefore ambient neutron and gamma-ray background) as low as possible. In the case of the full-energy beam, however, it was necessary to use the premagnet collimator as well as control of the internal beam, in order to obtain a reliable low-intensity beam in the experimental area.

3. Target and Counters

The target used in this experiment was an earlier version of the one described in detail in Chapter II. It contained 2.80 g/cm^2 liquid hydrogen with a total wall thickness of 0.35 g/cm^2 styrofoam. In all important features it was equivalent to the styrofoam target described earlier.

Counter No. 1 in this layout was the same as that used as counter No. 1 (see Chapter IIA3) in the small-angle experiment. In addition to forming part of the beam-defining system, this counter was used for its pulse-height resolution to detect the presence of very-low-energy particles in the incident beam.

Counter No. 2 consisted of plastic scintillator 1.74 by 1.74 cm^2 in area by 0.32 cm thick viewed by a 1P21 photomultiplier tube. The requirements for this counter were essentially the same, although not so severe, as those for the corresponding counter in the small-angle experiment.

Counter No. 3 was constructed of lucite containing terphenyl dissolved in phenylcyclohexane as a liquid scintillator. The active volume of the counter was disc-shaped, 8 inches in diameter by 1 inch thick, viewed by 7 type 5819 photomultipliers. Each of these photomultipliers was optically coupled through a small conical light pipe to a section of the lucite container. By adjustment of the relative voltages on the phototubes, the combined signal due to the traversal of a charged particle through the active volume could be made substantially independent of the position of the ionizing event in the counter.

4. Electronic and Photographic Setup

A block diagram of the electronics is shown in Fig. 13. In some

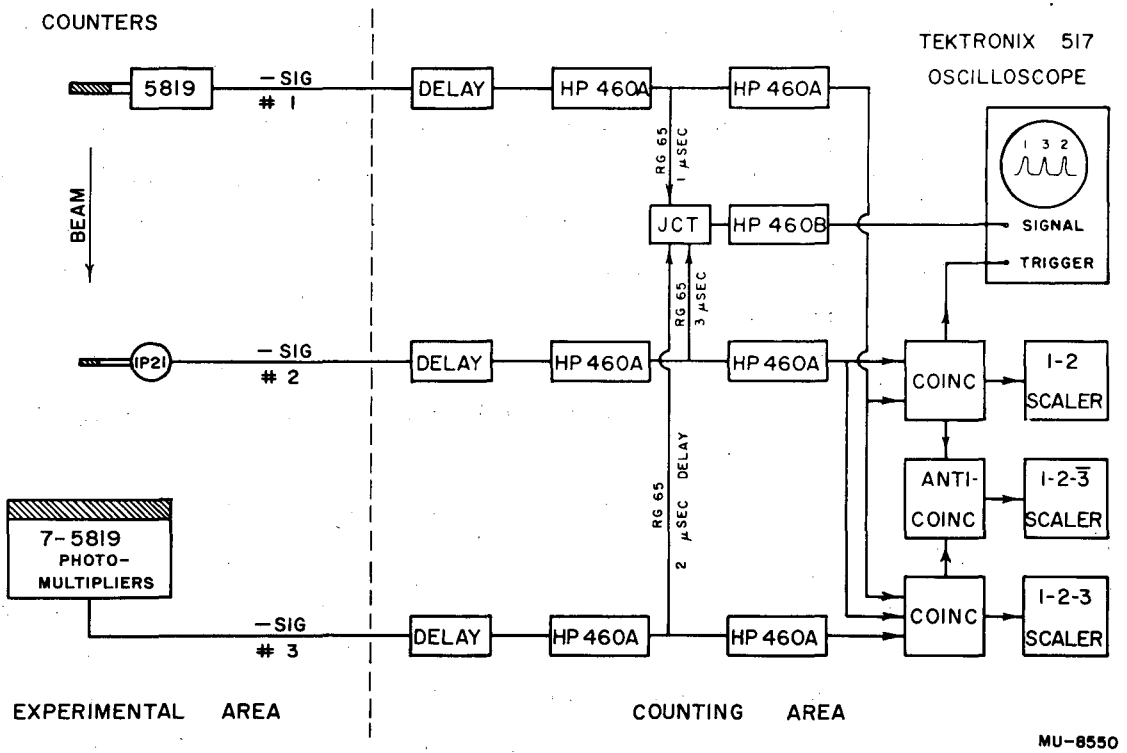


Fig. 13. Block diagram of electronics for attenuation experiment.

of the early runs the anticoincidence equipment was not available, but otherwise the electronics were connected substantially as shown for all runs. Hewlett-Packard type 460A distributed amplifiers were used between the counters and coincidence inputs. The coincidence circuits were of the Garwin³¹ type with a resolution of the order of 2×10^{-8} second and an input threshold of about one volt. The scalers were conventional with resolving times of about one microsecond.

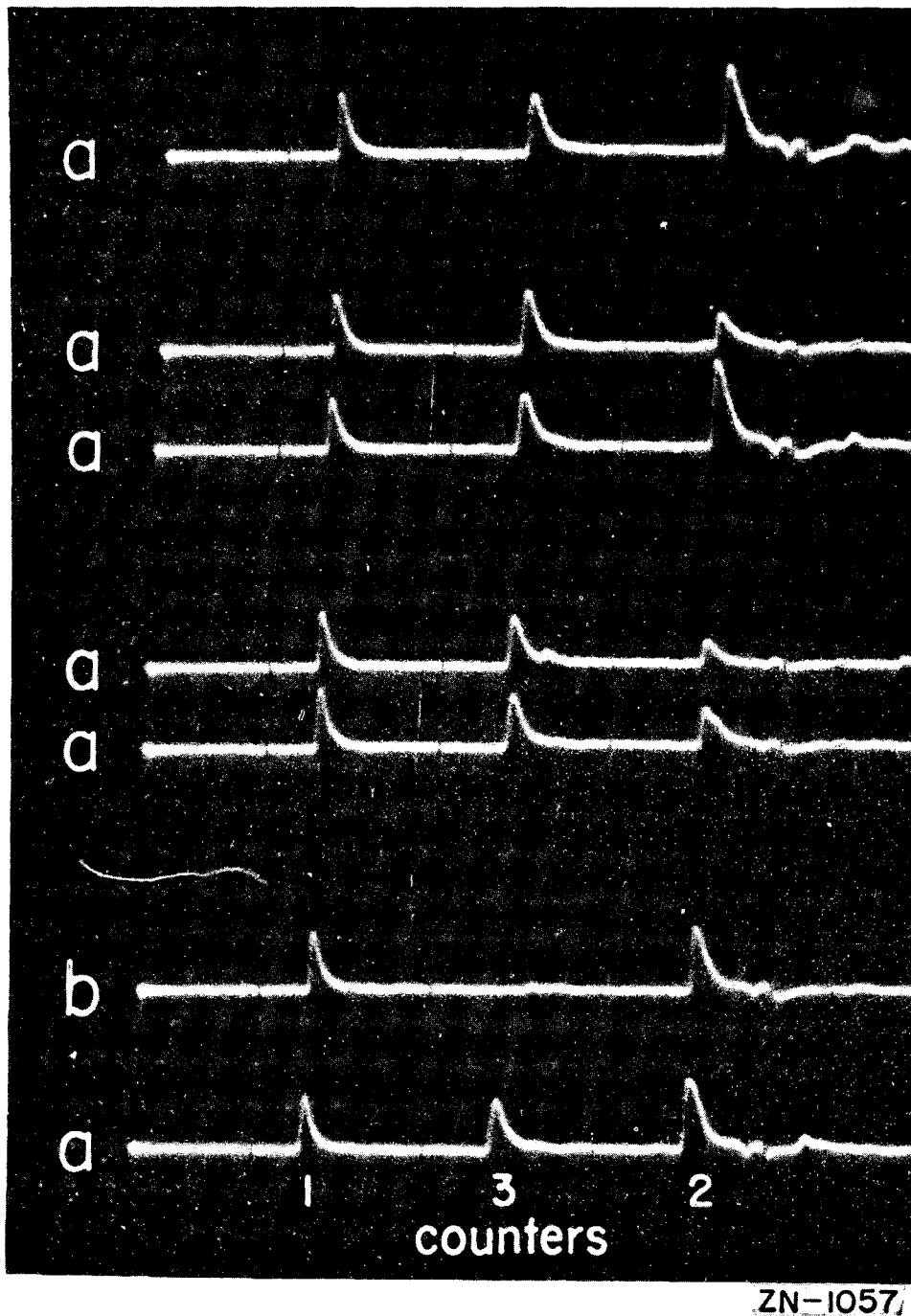
In addition to triggering the coincidence circuits, the signals from all three counters after amplification were tapped off into high-impedance RG65 delay cables of differing lengths. These three signals, delayed and separated in time by one microsecond, were then combined and fed to the vertical amplifier of a Tektronix type 517 oscilloscope. The internal amplifier in the oscilloscope broadened the pulses sufficiently to make them easily visible on the $1 \mu\text{sec}/\text{cm}$ sweep used. Part of the output of the 1-2 coincidence circuit was split off and used to trigger the oscilloscope sweep. The pulses were photographed on a continuously moving strip of 35 mm film in a General Radio camera. Figure 14 shows a typical section of film. With the 1-2 coincidence rate at about 4 per second, the film speed was adjusted to give approximately 50 sweeps per foot.

B. Procedure

1. Line-up

Line-up was accomplished with X-ray films in a manner similar to the small-angle experiment. After exposure and development the films were reproducibly replaced in fixed holders and the counters were brought into line by sighting through holes punched in the films at the center of the beam pattern.

Following the geometrical line-up of the equipment in the experimental area, the counters were brought into coincidence and the coincidence rate as a function of photomultiplier voltage for each counter was measured. Once the coincidence circuit threshold was reached, the counting rates were found to be independent of the voltage, within statistics. Since the alignment was accomplished with the full-energy beam, the larger pulses obtained from the counters when the beam energy was



ZN-1057

Fig. 14. Typical sweeps photographed from oscilloscope.

reduced assured that the desired pulses were being counted under all conditions of running.

2. Range Curves and Beam Homogeneity

The beam energy and homogeneity were checked by taking a range curve at each beam energy used. Figure 15 is a plot of $\frac{n(1-2-3)}{n(1-2)}$ for three energies as a function of copper absorber placed immediately in front of counter No. 3. The 1-2-3 counting rate is seen to fall off gradually at first owing to the nuclear absorption in the copper, and then to drop suddenly at the end of the particles' range. The behavior is in good agreement with the results of Kirschbaum.³⁶ The energies obtained from the range data (corrected for the counter thicknesses and target walls) using the range-energy tables of Aron et al.³⁴ are given next to each curve. They are in good agreement with the expected energies calculated from the known initial beam energy and the added internal absorber. The internal absorber used at each energy is indicated on the graph along with the optimum focus-magnet current.

As a further check on the homogeneity of the beam, sections of film from both the full-energy and the 240-Mev beam were scanned for pulse height from counter No. 1. A plot of the pulse-height distributions obtained is given in Fig. 16. The separation of the peaks of the two distributions is in agreement with the expected increase in specific ionization at the lower energy.

The main purpose of taking careful pulse-height measurements was to establish that counter No. 1 was able to distinguish clearly the presence of incident beam particles with less than 100 Mev of energy. At less than 100 Mev, an incident particle does not have sufficient range to penetrate the liquid hydrogen and count in the rear counter. Since the effect to be measured corresponds to an attenuation of roughly 4 percent, the absence of particles with energies less than 100 Mev must be established to a high degree of accuracy. These low-energy particles correspond to pulse heights greater than 2.2, 1.8, or 1.5 times the average pulse height at the energies 340, 240, and 175 Mev, respectively. Table IV lists the number of pulses found with heights greater than these values together with the number of sweeps viewed for each energy. As all the data shown were taken from films with the target in the hydrogen

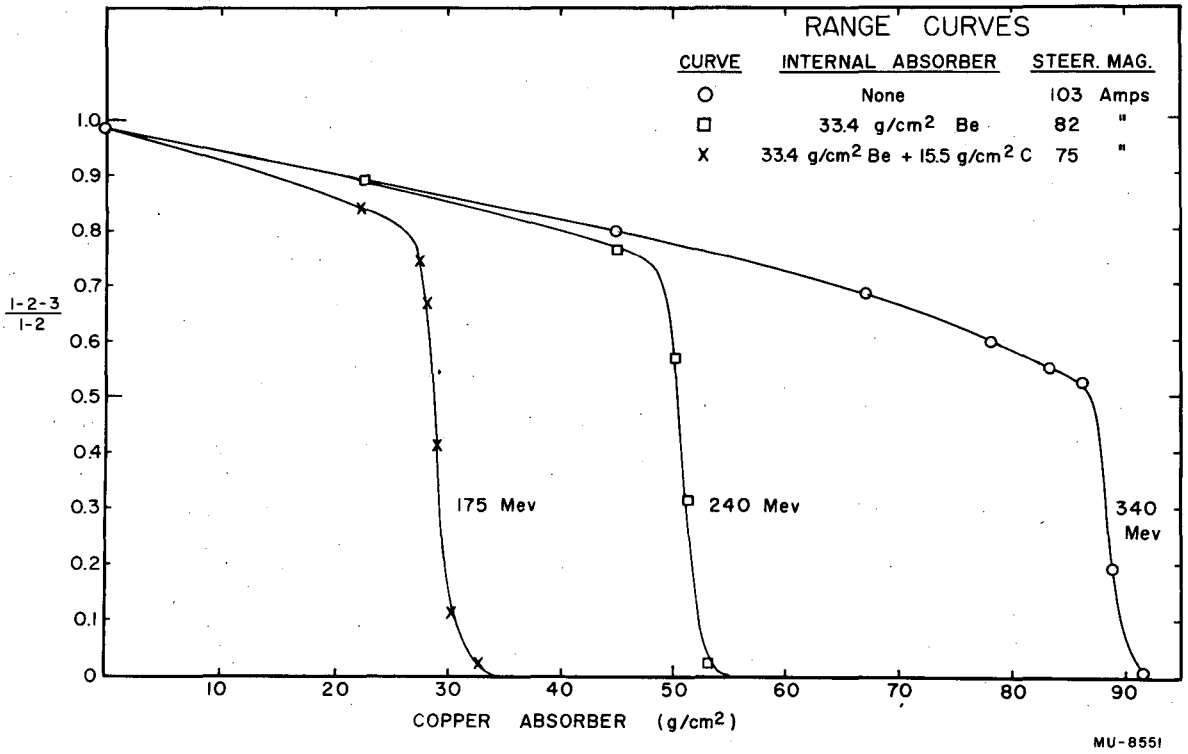


Fig. 15. Range curves for counter No. 3 at three energies

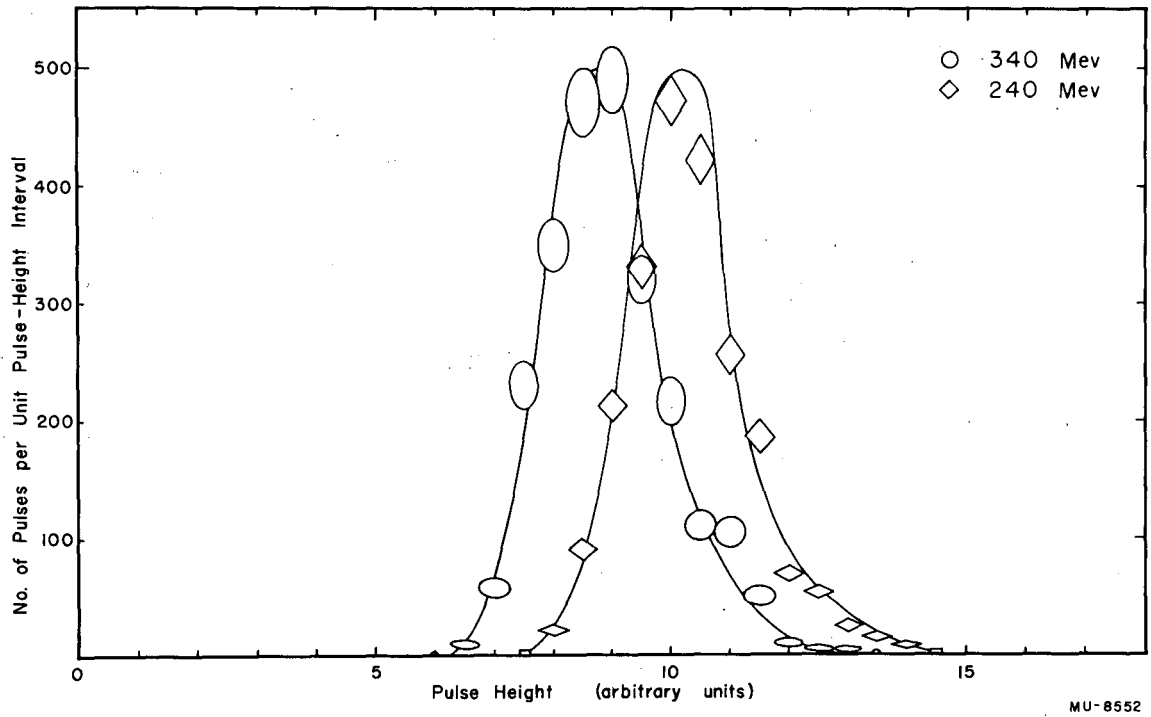


Fig. 16. Pulse-height spectrum taken from photographic data at two energies.

Table IV

| Incident Energy (Mev) | Sweeps Viewed | Pulses Corresponding to < 100-Mev Protons | No. per 1000 Incident Particles |
|-----------------------|---------------|---|---------------------------------|
| 340 | 5136 | 2 | 0.39 |
| 340 | 5395 | 5 | 0.93 |
| 340 | 5838 | 4 | 0.68 |
| 340 | 5296 | 4 | 0.75 |
| 340 | 5800 | 6 | 1.03 |
| 340 | 5645 | 3 | 0.53 |
| 340 total | 33110 | total 24 | average 0.72 ± 0.15 |
| 240 | 7804 | 2 | 0.26 |
| 240 | 5254 | 2 | 0.38 |
| 240 total | 13058 | total 4 | average 0.31 ± 0.15 |
| 175 | 4373 | 0 | 0.0 ± 0.23 |

position, it was further required that the large pulse height be associated with an apparent scattering or type "b" event. Thus the possibility of confusion with multiple-proton pulses was also eliminated.

3. Taking Data

The bulk of the data were taken at 1-2 counting rates below 10 per second. This was done primarily to allow separation of the traces photographed on moving film. Also, the early runs used conventional scalers of one microsecond resolution to determine directly the attenuated particles. Consequently, great emphasis was placed on counting every particle. Attenuation was determined by taking the difference: $n(1-2) - n(1-2-3)$.

In the later runs, however, which included all the 175-Mev data, a scaler having 10^{-2} -microsecond resolution and an electronic anti-coincidence unit were available. Some of the data were photographed at low counting rates to determine beam homogeneity as previously described, but for the majority of these runs the 1-2 counting rate was held at approximately 30 per second. The taking of sufficient film data to determine the hydrogen attenuation independently of the electronic measurements was not attempted in the runs for which the improved equipment was available.

Each cycle consisted of approximately 10 minutes of hydrogen data followed by 5 minutes of blank. This cycle was pursued until a sufficient amount of data was accumulated. Occasional data were also taken with the beam raised and lowered to ensure that the measured quantities were substantially independent of the counting rate.

In order to check whether the effect was strongly dependent on the value of θ_1 chosen (see Fig. 12), some data were taken with counter No. 3 pulled back slightly. If θ_1 is chosen sufficiently large to exclude scattering by Coulomb forces, and, in the full-energy case, the small-angle deuterons resulting from the reaction $p + p \rightarrow \pi^+ + d$, then the effect on the observed cross section of varying this cutoff angle should be slight.

C. Data Reduction and Errors

1. Reading the Film

Following the run, the film was developed and read. A standard

projection-type microfilm viewer was used to read the film. A typical section is shown in Fig. 14. In addition to identifying each event as type "a" (no scattering) or type "b" (scattering), large No. 1 pulses were measured to determine whether they fell into the suspect category of Table IV. The fraction of the incident beam that was scattered out was determined by dividing the type "b" events (equivalent to the electronic 1-2-3) by the type "a" plus "b" (electronic 1-2). Table V compares directly the results of reading the film with the electronic data taken in the same interval.

2. Calculations

- Let f_H, f_B = fraction of incident particles removed from the beam for the target plus hydrogen and the blank positions, respectively;
- g_H, g_B = opacity of the target for the hydrogen and blank positions, respectively;
- M = mass of neutral hydrogen atom = 1.6734×10^{-24} g,
- ρ = density of liquid hydrogen at one atmosphere and boiling point,
= 0.0709 g/cm^3 (Ref. 38);
- R = radius of counter No. 3 = 10.2 cm;
- t = thickness of hydrogen in target = 39.6 cm.

We note that

$$f = 1 - e^{-g}; \quad g = -\ln(1 - f), \quad (1)$$

and that

$$g_H - g_B = \frac{f_H - f_B}{1 - \frac{(f_H + f_B)}{2} - \frac{(f_H - f_B)^2}{12} + \dots},$$

$$\cong \frac{f_H - f_B}{1 - \frac{(f_H + f_B)}{2}} \quad (2)$$

is a sufficiently good approximation in this case.

Since it is known that for all the beam energies involved in the present experiment the differential scattering cross section is the same at all angles ($20^\circ < \theta < 90^\circ$)^{1, 3-5}, the results of an attenuation experiment may be expressed in terms of the differential cross section rather than in terms of the total scattering cross section.

It is shown in Appendix F that the center-of-mass differential-scat-

Table V

| θ_1 | Incident Beam Energy | Method | f_H | f_B | $f_H - f_B$ |
|------------|----------------------------|--------------|-----------------|-----------------|-----------------|
| degrees | Mev | | % | % | % |
| 6.3 | 340 | Electronic | 5.03 ± 0.17 | 1.41 ± 0.12 | 3.62 ± 0.20 |
| 6.3 | 340 | Photographic | 5.06 ± 0.17 | 1.44 ± 0.12 | 3.62 ± 0.20 |
| 7.4 | 340 | Electronic | 4.53 ± 0.14 | 1.14 ± 0.11 | 3.39 ± 0.18 |
| 7.4 | 340 | Photographic | 4.75 ± 0.15 | 1.33 ± 0.12 | 3.42 ± 0.19 |
| 7.4 | 240 | Electronic | 4.51 ± 0.15 | 1.16 ± 0.10 | 3.35 ± 0.18 |
| 7.4 | 240 | Photographic | 4.72 ± 0.16 | 1.34 ± 0.11 | 3.37 ± 0.20 |

tering cross section averaged over scattering angle is equal to

$$\overline{\left(\frac{d\sigma}{d\omega}\right)_{\text{c.m.}}} = \frac{M\Delta g}{2\pi\rho t} \left[1 - \frac{2R}{t} (\phi_2 - \phi_1) \right]^{-1}, \quad (3)$$

where Δg is the opacity of the liquid hydrogen = $g_H - g_B$, and ϕ_1 and ϕ_2 are shown in Fig. 5B.

Inserting Eq. (2) into Eq. (3), we have the desired relation for computing $\overline{\left(\frac{d\sigma}{d\omega}\right)_{\text{c.m.}}}$:

$$\overline{\left(\frac{d\sigma}{d\omega}\right)_{\text{c.m.}}} = \frac{M(f_H - f_B)}{2\pi\rho t} \left\{ \left[1 - \frac{1}{2} (f_H + f_B) \right] \left[1 - \frac{2R}{t} (\phi_2 - \phi_1) \right] \right\}^{-1}. \quad (4)$$

The total cross section for scattering through an angle greater than 20° c.m. is then given by

$$\sigma_{>20^\circ} = 2\pi \overline{\left(\frac{d\sigma}{d\omega}\right)_{\text{c.m.}}} \int_{20^\circ}^{90^\circ} \sin\theta d\theta = 2\pi \cos(20^\circ) \overline{\left(\frac{d\sigma}{d\omega}\right)_{\text{c.m.}}} \quad (5)$$

Table VI lists the uncorrected results of the various runs and includes all the electronic data taken. The errors shown are those arising from counting statistics only.

3. Corrections

There are three small corrections to be applied to the measured cross sections:

a. Hydrogen gas above liquid hydrogen. When taking blank data by lowering the target assembly containing liquid hydrogen, we must correct the blank data for the cold hydrogen gas in the path of the beam in the blank position. Assuming that the hydrogen gas immediately above the liquid hydrogen is still at the same temperature, the ratio of densities³⁸ is $\frac{1.33}{70.9} = 0.019$. Thus the difference ($f_H - f_B$) is due to an amount of hydrogen 1.9 percent less than that contained in the target. The calculated cross sections should be increased by 1.9 percent.

b. Pile-up in counter No. 3. If more than one proton traverses the target during the resolution time of the 1-2-3 coincidence system, a scattering event involving one proton will not be observed. Appendix A, Eq.

Table VI

| Incident Beam Energy | Approx. 1-2 Ctg. Rate | $\phi_2 - \phi_1$ | f_H | f_B | uncorrected $\left(\frac{d\sigma}{d\omega}\right)$ c.m. | uncorrected $\sigma_{>20^\circ}$ |
|----------------------------|-----------------------------|-------------------|-------------|-------------|---|-------------------------------------|
| Mev | second ⁻¹ | radians | % | % | mb/steradian | millibarns |
| 340 | 4 | 0.079 | 4.90 ± 0.10 | 1.26 ± 0.07 | 3.72 ± 0.12 | 22.0 ± 0.7 |
| 340 | 4 | 0.114 | 4.65 ± 0.10 | 1.05 ± 0.07 | 3.74 ± 0.12 | 22.1 ± 0.7 |
| 340 | 30 | 0.114 | 5.04 ± 0.11 | 1.36 ± 0.07 | 3.83 ± 0.13 | 22.6 ± 0.8 |
| 240 | 4 | 0.114 | 4.55 ± 0.09 | 1.14 ± 0.07 | 3.55 ± 0.12 | 21.0 ± 0.7 |
| 175 | 3 | 0.114 | 5.50 ± 0.19 | 1.71 ± 0.13 | 3.97 ± 0.24 | 23.4 ± 1.4 |
| 175 | 30 | 0.114 | 5.57 ± 0.09 | 1.70 ± 0.06 | 4.06 ± 0.11 | 24.0 ± 0.7 |

(2), shows a fraction $\frac{N\tau}{2} (2a + 1)$ of the 1-2 counting rate to be so afflicted, where N is the true counting rate in counter No. 2 and $(1 + a)N$ is the true counting rate in counter No. 3. The quantity "a" was measured by comparing the single rate in counter No. 3 (tested to make sure that all counts were beam-derived) to the 1-2 counting rate. A value of 3 was obtained for "a". Using $\tau = \frac{1}{W}$, where W is the number of resolving times per second, here equal to the number of fine-structure windows in the beam per second, we obtain $\tau = 10^{-4}$ seconds.³³ Thus the data taken at thirty 1-2 counts per second suffered approximately 1 percent pileup in counter No. 3, i. e. 1 percent of the actual scattering events were not seen. The net fraction by which the calculated cross section should be increased is thus 1 percent at $N = 30$ per second, and by a negligible amount at 4 per second.

It is interesting to note that the calculated accidental rate (Eq. 3 of Appendix A), between counter No. 3 and the 1-2 coincidences, agrees closely with that measured by inserting 6×10^{-8} second delay in the pulses from counter No. 3. Thus the value $W = 10^4$ per second seems a reasonable one in the present case.

c. Contamination by Low-energy Particles. Referring to Table IV, we see that the contamination of the primary beam by particles of less than 100 Mev varies between 0 and 7×10^{-4} . Thus a negative correction of $\frac{C}{(f_H - f_B)}$, where C is the fractional contamination of the beam, seems indicated. Downward corrections of 2, 1 and 0 percent were applied to the 340-, 240-, and 175-Mev data, respectively. Since these numbers are poorly determined statistically, the over-all error must be increased accordingly.

The remaining correction applies to the energy at which the results are quoted. At 340, 240, and 175 Mev, the beam loses 20, 24, and 30 Mev,³⁴ respectively, in traversing the liquid hydrogen in the target. Therefore, the results are quoted for mean energies of scattering in the laboratory system. These have been rounded to 330, 230, and 160 Mev, respectively.

4. Errors

a. Statistical Errors. The statistical error arising from counting fluctuations was assumed to follow a Poisson law. The values given are in terms of standard deviation. The error due to fluctuations in the low-energy pulses has been set at 1 percent. The statistical errors have been combined by taking the root mean square of the individual contributions. They are seen to be in the vicinity of 3 percent.

b. Systematic Errors. The chief systematic error is thought to arise in the determination of the target thickness. The dimensional measurements are good to about 2 millimeters out of 396, or better than 1 percent. However, the behavior of styrofoam under severe cooling is not well known. The external dimensions of the liquid hydrogen container were observed not to change radically under cooling and the target did not break, so there could have been no drastic changes in the length of the hydrogen path. In addition, the change in the length of the nickel liner could be calculated as 0.002 and since no damage was done by the target's shrinking around this tight-fitting insert, it is felt that target shrinkage did not exceed 1 percent. In view of the lack of knowledge, however, an error of -2 percent has been given this quantity, leading to a positive uncertainty of 2 percent in the cross section.

The uncertainties in the measurement of the other quantities in the system have a negligible effect on the cross section. The weighted averages for the results at each energy, containing the corrections and errors discussed in this section, are shown in Table VII.

Table VII

| Mean Energy | corrected $\sigma_{>20^\circ}$ | corrected $\left(\frac{d\sigma}{d\omega}\right)_{\text{c.m.}}$ |
|-------------|-----------------------------------|---|
| Mev | millibarns | mb/steradian |
| 330 | + 0.9 | + 0.15 |
| | 22.5 | 3.81 |
| 230 | - 0.4 | - 0.07 |
| | + 1.1 | + 0.19 |
| 160 | 21.2 | 3.58 |
| | - 0.7 | - 0.12 |
| 160 | + 1.1 | + 0.19 |
| | 24.5 | 4.16 |
| | - 0.6 | - 0.10 |

IV. DISCUSSION

A. Small-Angle Cross Section

For a collision between identical particles of unit charge, the correct Rutherford (or Coulomb) scattering cross section is given by

$$\left(\frac{d\sigma}{d\omega}\right)_{\text{c.m.}} = \left(\frac{\eta\lambda}{2}\right)^2 \left\{ \frac{1}{\sin^4(\theta/2)} + \frac{1}{\cos^4(\theta/2)} - \frac{4 \cos [2\eta \ln \tan(\theta/2)]}{\sin^2 \theta} \right\},$$

where $2\pi\lambda =$ de Broglie wave length in the center-of-mass system.

$$\eta = \frac{e^2}{hv}; \quad v = \text{relative velocity in the } \underline{\text{laboratory}} \text{ system.}$$

$\theta =$ center-of-mass scattering angle.

For angles sufficiently small so that $\sin(\theta/2) \approx \theta/2$, the cross section may be approximated by

$$\left(\frac{d\sigma}{d\omega}\right)_{\text{c.m.}} \approx \left[\left(\frac{e^2}{Mc^2}\right) \frac{2}{\gamma'\beta'\beta} \right]^2 \frac{1}{\theta^4},$$

where $\frac{e^2}{Mc^2} =$ "classical" proton radius $= 1.5350 \times 10^{-16}$ cm;

$$\gamma' = \frac{1}{\sqrt{1 - \beta'^2}}; \quad \beta'c = \text{center-of-mass velocity};$$

$\beta c =$ relative particle velocity in laboratory system.

Figure 17 shows the results of Chapter II together with a logarithmic plot of the theoretical Coulomb scattering cross section plus a nuclear contribution assumed constant at 3.75 mb/steradian. No interference is included. There seems to be an indication of destructive interference, but this is less marked than in the results of Fischer and Goldhaber.¹⁰ The nuclear part of the proton-proton scattering cross section appears to remain constant within ± 5 percent until the Coulomb term dominates.

These two features of the cross section--its constancy with angle and the destructive interference observed in the Coulomb scattering region--can be fitted using only S and P partial-wave phase shifts. Thaler

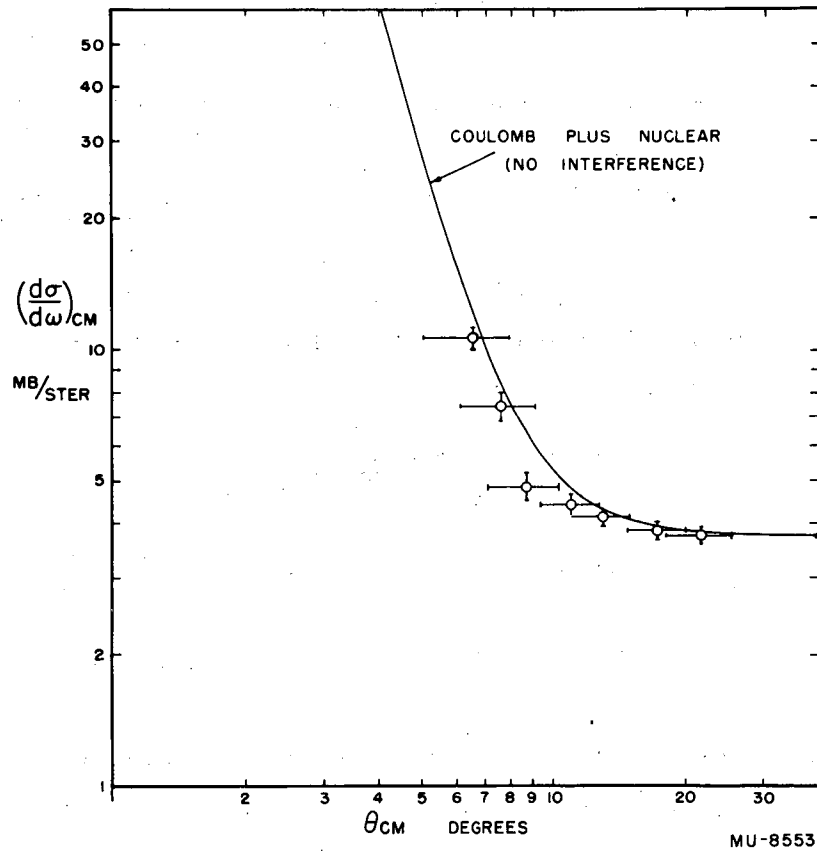


Fig. 17. Plot of experimental differential p-p cross section as a function of center-of-mass scattering angle. The solid curve is a sum of the theoretical Coulomb cross section and an assumed constant value. This constant value has been taken equal to the cross section at large angles, 3.75 mb/steradian.

and Bengston²¹ have made a phase-shift analysis of the 240-Mev data of Towler,⁵ using only S and P waves without benefit of a potential assumption. At that energy, they find a definite constructive interference between the Coulomb and nuclear terms. To this extent we are in disagreement with the 240-Mev results. Fried³⁹ has shown that Thaler and Bengston's phase shifts are also not compatible with the recent polarization results of Chamberlain, Segrè, Tripp, Wiegand, and Ypsilantis.²³

B. Small-Angle Polarization

If we assume the interaction between two particles to be invariant under simultaneous rotation of both space and spin coordinates, then for spin-1/2 particles whose polarization (expectation value of spin) may be described by a pseudovector,⁴⁰ the polarization produced by the scattering of an unpolarized beam on an unpolarized target must be given by $\hat{n}P(\theta)$, where \hat{n} is a unit vector perpendicular to the plane of scattering. Thus we see that the polarization at θ , $\theta + \pi$, must be oppositely directed to that at θ , θ , or

$$P(\theta, \theta) = -P(\theta, \theta + \pi) \quad (1)$$

In the case of proton-proton scattering, the quantum-mechanical indistinguishability of the particles imposes the additional restriction that the polarization be antisymmetric around 90° :

$$P(\theta) = -P(\pi - \theta) \quad (2)$$

If we now seek a Fourier expansion of the polarization,

$$P(\theta) = \sum_{n=0}^{\infty} (a_n \sin n\theta + b_n \cos n\theta),$$

we note that Eq. (1) requires all $b_n = 0$. Equation (2) requires that

$$a_n \sin n\theta = -a_n \sin n(\pi - \theta) = (-1)^n a_n \sin n\theta.$$

therefore, $a_n = 0$ for n odd. Thus we may write as the most general expression for proton-proton polarization

$$P(\theta) = a_2 \sin 2\theta + a_4 \sin 4\theta + a_6 \sin 6\theta + \dots$$

Expanding and regrouping terms gives

$$P(\theta) = \sin \theta \cos \theta (a_0 + a_2 \cos^2 \theta + a_4 \cos^4 \theta + \dots)$$

Comparing this result with an expansion in terms of partial waves, we find that the highest-order coefficient, a_{2n} , needed to fit the observed data is a measure of the number of partial waves entering into the interaction. Coulomb effects, of course, introduce many higher-order terms at very small angles, but these should be small at angles greater than 15° center-of-mass.

Figure 18 is a plot of $P(\theta)/\sin \theta \cos \theta$ versus $\cos^2 \theta$. Previous data of Chamberlain et al^{23, 26} at the same energy have been included. The straight line is a least-squares fit assuming the presence only of a_0 and a_2 . The present experimental statistics do not seem to require a_4 , but are certainly not good enough to exclude a substantial $\cos^4 \theta$ contribution. Since the cross section is substantially constant for angles greater than 15° c. m. $\sigma(\theta)P(\theta) = \text{const } P(\theta)$, and it may be shown that the exclusion of a_4 corresponds to an upper limit of 3F_2 and 3F_3 , but no 3F_4 or higher partial waves. The presence of a_2 demands the presence of at least one 3F wave in the scattering. These 3F waves may arise from mixing with a 3P wave via a tensor-force potential, or may be directly excited from a spin-orbit interaction.

Referring to Figs. 10 and 18, we note that the experimental data suggest a deviation from a simple $\sin \theta \cos \theta (a_0 + a_2 \cos^2 \theta)$ behavior at small angles. As mentioned previously, this is to be expected because of the presence of higher-order partial waves from the Coulomb (charge and magnetic moment) interaction. Several authors⁴⁶ have derived the explicit form which the polarization (and cross section) will take in this angular region, assuming only S and P waves are involved in the nuclear interaction. The evidence here indicates that D and F waves should also be included.

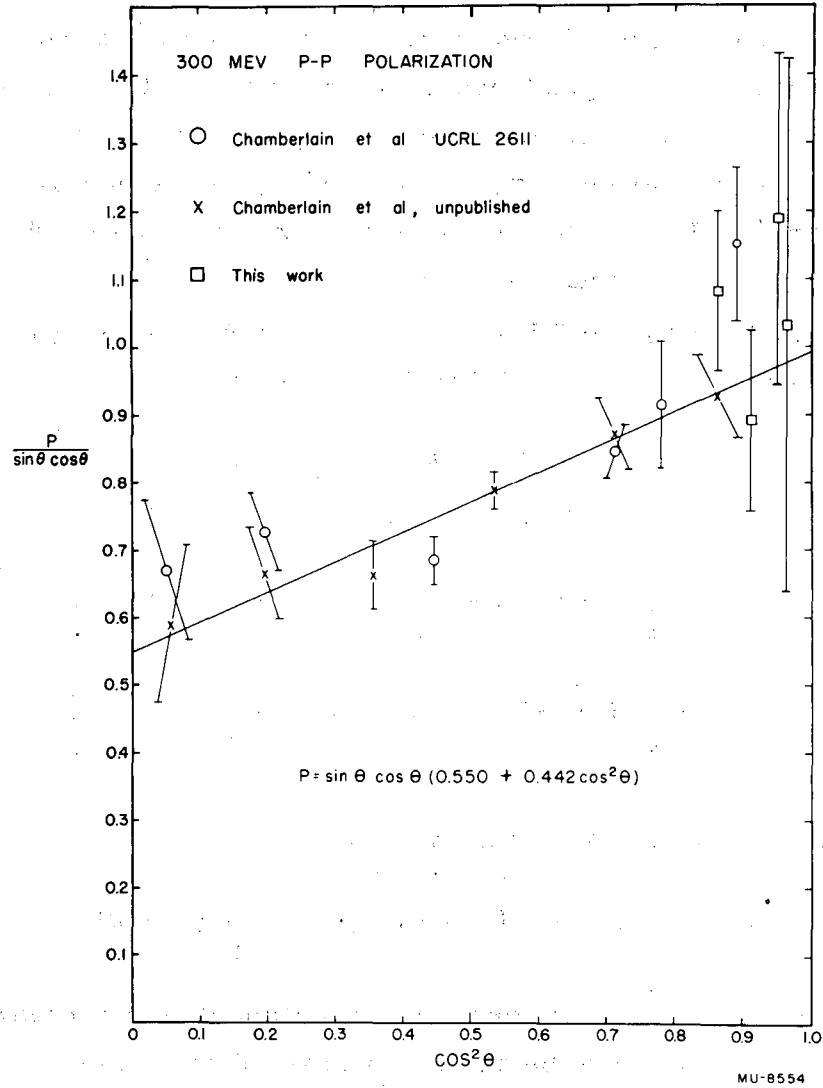


Fig. 18. $P(\theta)/\sin \theta \cos \theta$ vs $\cos^2 \theta$ including large-angle results. The solid line is a least-squares fit to the data, given by the equation shown.

C. Attenuation Cross Section and the Charge-Independent Inequality

When dealing with a system which we suspect may possess charge-independent properties, it is convenient to employ the concept of isotopic spin. This formalism assigns an isotopic total spin $\tau = 1/2$ to a nucleon; the "z" component $\tau_3 = +1/2$ representing a proton, $\tau_3 = -1/2$ a neutron. The charge-independent nature of a reaction may then be related to the independence of the reaction to the orientation of the total isotopic spin, τ (i. e., it should depend only on the total isotopic spin). The conservation of τ_3 is, of course, demanded by conservation of charge. The mathematical structure involved is identical with that developed for ordinary-spin space.

Writing down the possible nucleon-nucleon systems in isotopic-spin space, we have (after symmetrizing)

$$\begin{array}{llll}
 \uparrow\uparrow & = & \text{p-p} & : f_1 \\
 \downarrow\downarrow & = & \text{n-n} & : f_2 \\
 \frac{1}{\sqrt{2}} (\downarrow\uparrow + \uparrow\downarrow) & = & \frac{1}{\sqrt{2}} (\text{n-p} + \text{p-n}) & : f_3 \\
 \frac{1}{\sqrt{2}} (\downarrow\uparrow - \uparrow\downarrow) & = & \frac{1}{\sqrt{2}} (\text{n-p} - \text{p-n}) & : g
 \end{array}
 \left. \begin{array}{l} \\ \\ \\ \end{array} \right\} \begin{array}{l} \text{isotopic-spin} \\ \\ \text{triplet, } = 1 \\ \\ \text{isotopic-spin} \\ \text{singlet, } = 0. \end{array}$$

Solving for n-p and p-n, we have

$$\text{n-p} = \frac{1}{\sqrt{2}} (f_3 + g) ; \text{p-n} = \frac{1}{\sqrt{2}} (f_3 - g) .$$

Forming cross sections (assuming space and ordinary-spin parts of the scattered wave to be absorbed in f and g) we have

$$\begin{aligned}
 \sigma_{pp} &= 2 |f_1|^2 \\
 \sigma_{nn} &= 2 |f_2|^2 \\
 \sigma_{np} &= \frac{1}{2} |f_3 + g|^2 = \frac{1}{2} |f_3|^2 + \frac{1}{2} |g|^2 + \text{Re } f_3^* g \\
 \sigma_{pn} &= \frac{1}{2} |f_3 - g|^2 = \frac{1}{2} |f_3|^2 + \frac{1}{2} |g|^2 - \text{Re } f_3^* g
 \end{aligned}$$

If the nucleon-nucleon scattering is to be charge-independent, we must have $f_1 = f_2 = f_3$, and therefore

$$\sigma_{np} + \sigma_{pn} = |f|^2 + |g|^2 \geq |f|^2 = \sigma_{pp}/2 = \sigma_{nn}/2 .$$

From the kinematics of the reaction, we know that $\sigma_{np}(\theta) = \sigma_{pn}(\pi - \theta)$. For a pair of reactions, therefore, that display charge independence, the following inequality must be obeyed:

$$\sigma_{np}(\theta) + \sigma_{np}(\pi - \theta) \geq \sigma_{pp}(\theta)/2 .$$

The most stringent test of this inequality comes at $\theta = 90^\circ$, where σ_{np} is observed to be smallest. At 90° we must have

$$\frac{\sigma_{pp}}{\sigma_{np}} \leq 4 .$$

The average value for the differential proton-proton cross section obtained in Chapter III is plotted against energy in Fig. 19, along with the 90° results of other laboratories. Also plotted is $4\sigma_{np}(90^\circ)$ obtained from various sources. Since the dotted ($4\sigma_{np}$) line does not drop below the solid (σ_{pp}) line, we see that the inequality restriction is not violated.

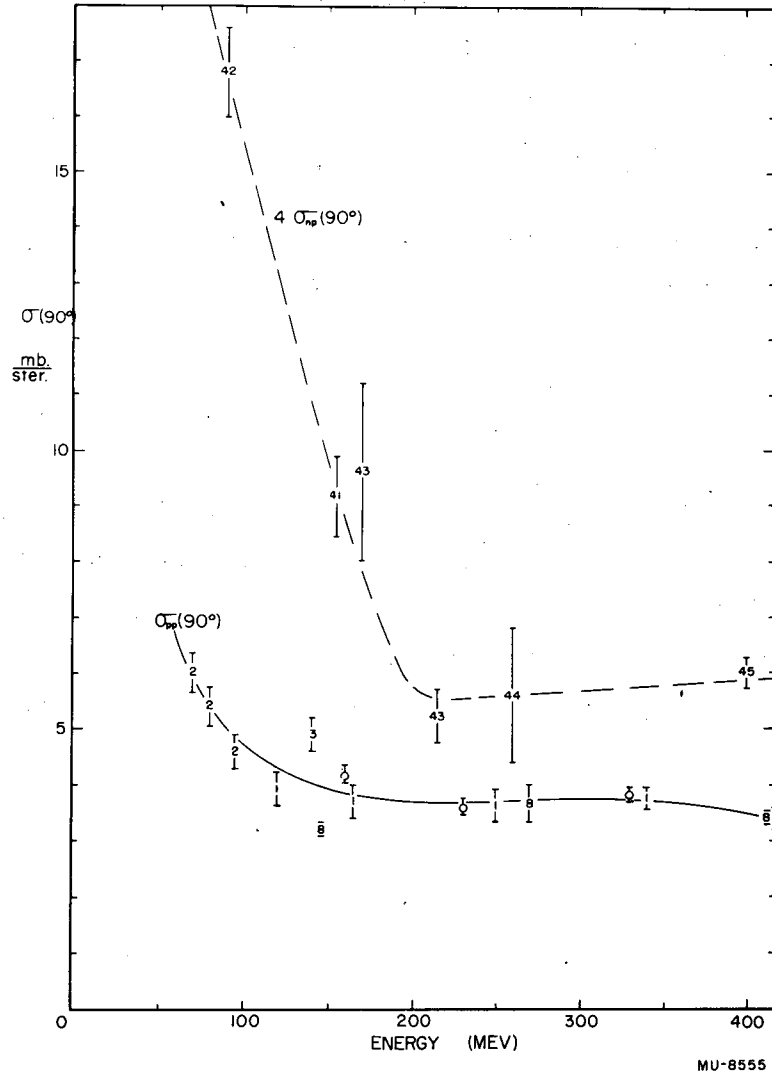


Fig. 19. Ninety-degree p-p (solid line) and n-p (dotted line) differential scattering cross sections as a function of energy. The numbers give the reference from which the value was taken; the circles represent the values obtained in Chapter III.

V. CONCLUSION

In view of the complicated nature of the Coulomb-nuclear interference terms it would seem natural to attempt calculation of the partial-wave phase shifts on the basis of purely nuclear (non-Coulomb) effects. These would include the large-angle cross section, polarization, and the more esoteric results of recent triple-scattering data. In principle, at least, these could determine the values and relative signs of all nuclear phase shifts. The resulting ambiguity in absolute sign might then be resolved by computing the predicted interference terms for the two possible choices and comparing them with the small-angle polarization and cross-section data in the Coulomb-nuclear interference region.

Unfortunately, the estimated errors in the polarization data become large at just the angles where interference is most pronounced. There is hope, however, that the larger-angle experiments referred to above may be sufficiently determinate to narrow the choice to perhaps two grossly different interference effects. It is possible that using both the small-angle cross section and polarization data, will permit a clear-cut choice to be made. If so, it is interesting to note that the direction of the polarization and the attractive or repulsive nature of the spin-dependent forces operating can be determined from the theoretically well-known characteristics of the Coulomb interaction.

It appears that the hypothesis of charge independence is still on solid ground.

VI. ACKNOWLEDGMENTS

The author wishes to express his sincere appreciation for the continuous advice and guidance of Professor Owen Chamberlain. Professor Emilio Segrè provided assistance and many helpful suggestions. Dr. Clyde Wiegand designed and constructed much of the novel electronic equipment used, and gave invaluable assistance during runs. The target and some of the auxiliary equipment were constructed by Mr. David Fischer, whose interested help was very much appreciated.

The author is grateful for many valuable discussions, particularly in connection with polarization, held with Messrs. Thomas Ypsilantis and Robert Tripp, and for the assistance they have rendered in setting up the polarized proton beam. Thanks are due the cyclotron crew under Mr. James Vale, which was at all times cooperative.

This work was performed under the auspices of the United States Atomic Energy Commission.

APPENDICES

A. Pile-up and Accidentals

Let τ be the effective resolving time of system ($\frac{1}{\tau}$ equals the number of resolvable intervals per second). Let N be the true counting rate. Then the Poisson Law gives, for the probability of x events within one resolving time,

$$P_x = \frac{(N\tau)^x}{x!} e^{-N\tau}$$

If $N\tau \ll 1$, then the observed counting rate, $n \cong \frac{P_1}{\tau} \cong N(1 - N\tau)$, and the number of pile-ups

$$\frac{P_2}{\tau} \cong \frac{N^2\tau}{2} (1 - N\tau)$$

The fraction of the observed counting rate that represents pile-ups is then

$$\cong \frac{N\tau}{2} \quad (1)$$

Suppose we have a system of two counters in coincidence, one of which, A, sees all the events N that happen in another, B, but which, in addition, sees aN uncorrelated events that B does not. Then the fraction of the observed AB coincidence counting rate, n , that corresponds to pile-up in counter A is equal to (pile-up in A minus pile-up in A but no event in B)/ n ,

$$\cong \frac{N\tau}{2} \left[(a+1)^2 - a^2 \right] = \frac{N\tau}{2} (2a+1) \quad (2)$$

If now all the events in counter A are uncorrelated with respect to B, but the rates are unchanged, then the fraction of the B rate that represents accidental AB coincidences will be

$$(AB)_{acc} \cong (a+1) N\tau \quad (3)$$

B. Small-angle Scattering Geometry

Referring to Fig. 5A, we have

$$\frac{\text{counts}}{\text{incid. protons}} = \left(\frac{d\sigma}{d\Omega} \right)_{\text{av}} \frac{\rho}{M} \int_{d-t/2}^{d+t/2} \Omega(x) dx,$$

where

$$\Omega(x) = \frac{Ax}{(x^2 + a^2)^{3/2}} \cong \frac{A \cos(H)}{x^2 + a^2},$$

$$H = \tan^{-1} \frac{a}{d},$$

$$a = 5.5 \text{ inches},$$

$$A = 28.9 \text{ (inches)}^2,$$

$$t = 15.6 \text{ inches},$$

$$\rho = 0.0709 \text{ g/cm}^3,$$

$$M = 1.6734 \times 10^{-24} \text{ g} = \text{mass of neutral H atom};$$

but

$$\int_{d-t/2}^{d+t/2} \frac{dx}{a^2 + x^2} = \frac{1}{a} \left[\tan^{-1} \left(\frac{x}{a} \right) \right]_{d-t/2}^{d+t/2} = \frac{1}{a} \tan^{-1} \frac{at}{a^2 + d^2 - (t/2)^2}$$

and

$$\left(\frac{d\sigma}{d\Omega} \right)_{\text{avg}} = \eta \frac{I_{\text{scat}}}{I_0},$$

$$\text{where } \eta = \frac{Ma}{\rho A \cos(H)} \left[\tan^{-1} \frac{at}{a^2 + d^2 - (t/2)^2} \right]^{-1}$$

$$\cong \frac{M}{\rho t A \cos(H)} \left[a^2 + d^2 - \left(\frac{t}{2} \right)^2 \right],$$

C. Angular Resolution for Small-Angle Experiment

The expression for the rms angle of multiple scattering may be put in the form

$$\delta(H)^2 \cong (Z+1) \frac{m}{M} \frac{\Delta E}{E},$$

- where Z = atomic number of scattering nuclei,
 M = mass of scattered particles,
 m = electronic mass,
 ΔE = energy loss in the scattering material,
 E = average energy of particle.

The rms angular deviation from the average angle of scattering, ϕ_0 , when a finite solid angle for scattering is subtended is given by

$$\overline{\delta \phi^2} = \frac{1}{\phi_{\max} - \phi_{\min}} \int_{\phi_{\min}}^{\phi_{\max}} f(\phi) (\phi - \phi_0)^2 d\phi, \text{ where } f(\phi) \text{ is a suitable distribution function.}$$

Referring to Fig. 5A, one may see that this reduces to (assuming $f(\theta) = \text{const.}$)

$$\begin{aligned} \overline{\delta \textcircled{H}}^2 &\cong \frac{W^2}{12d^2} \text{ for counter No. 3 (} W = \text{radial width of counter) ;} \\ &\cong \frac{t^2 \sin^2 \textcircled{H}}{12d^2} \text{ for the finite extension of the target,} \\ &= \frac{t^2 a^2}{12d^4} \text{ since } \sin \textcircled{H} \cong \frac{a}{d} ; \\ &= \frac{b^2}{12d^2} \text{ for the finite diameter of the beam} \\ &\hspace{15em} (b = \text{beam diameter}). \end{aligned}$$

Table VIII
 Angular Resolution, $\delta \textcircled{H}^2$, From
 Various Contributing Sources

| \textcircled{H} lab Degrees | Liq. H ₂ | Ctr. No. 1 | Ctr. No. 3 | Tgt. | Beam | $\Sigma \delta \textcircled{H}^2_{\text{lab}}$ |
|----------------------------------|------------------------|--|--|------|------|--|
| | | Units of 10^{-5} (\textcircled{H} in radians) | | | | |
| 3.0 | 7.9 | 4.5 | 0.76 | 0.51 | 0.38 | 14.1 |
| 3.5 | 7.9 | 4.5 | 0.97 | 0.88 | 0.49 | 14.8 |
| 4.0 | 7.9 | 4.5 | 1.34 | 1.58 | 0.67 | 16.0 |
| 5.0 | 7.9 | 4.5 | 2.1 | 3.9 | 1.05 | 19.5 |
| 6.0 | 7.9 | 4.5 | 3.0 | 8.0 | 1.5 | 24.9 |
| 8.0 | 7.9 | 4.5 | 5.3 | 24.8 | 2.7 | 45.2 |
| 10.0 | 7.9 | 4.5 | 8.3 | 60.5 | 4.2 | 85.4 |
| | Multiple Scattering | | Finite Width or Length of Elements of Geometry | | | TOTAL |

D. Asymmetry for Counter of Finite Extent

If we assume the counting rate per unit solid angle in counter No. 3 is given by

$$f(\theta) (1 + e \cos \phi),$$

where

θ is polar angle of scattering,

ϕ is azimuthal angle of scattering,

then the counting rate in the east (+) and west (-) halves of counter No. 3 will be given by

$$I_{\pm} = 2 \int_0^{\Delta\phi} f(\theta)(1 \pm e \cos \phi) d\phi = 2f(\theta)(\Delta\phi \pm e \sin \Delta\phi),$$

where $2\Delta\phi$ is the azimuthal angular span of either half of the counter. The measured asymmetry is then defined by

$$e' = \frac{I_+ - I_-}{I_+ + I_-} = e \frac{\sin \Delta\phi}{\Delta\phi}$$

E. Error in Asymmetry Due to Misalignment

If the asymmetry is given by

$$e = \frac{\sigma(\theta, 0) - \sigma(\theta, \pi)}{\sigma(\theta, 0) + \sigma(\theta, \pi)},$$

then direct calculation shows that an angular error $\delta\theta$ at azimuthal inclination ϕ in alignment of the beam with the zero of angular measurement gives

$$\delta e = \frac{2[\sigma(\theta, 0) \sigma'(\theta, \pi) + \sigma(\theta, \pi) \sigma'(\theta, 0)]}{[\sigma(\theta, 0) + \sigma(\theta, \pi)]^2} \cos \phi \delta \theta,$$

where the prime indicates derivative with respect to θ . In the region of Coulomb scattering, this reduces to

$$\delta e = \frac{16[\sigma(\theta, 0) \sigma(\theta, \pi)]}{[\sigma(\theta, 0) + \sigma(\theta, \pi)]^2} \cos \phi \frac{\delta\theta}{\theta} \cong 4 \cos \phi \frac{\delta\theta}{\theta},$$

if the true asymmetry is small, i. e. if $\sigma(\theta, 0) \cong \sigma(\theta, \pi)$.

F. Geometry for Attenuation Experiment

Referring to Fig. 5B, we see that the differential opacity of the target is given by

$$dg = \frac{\rho}{M} \sigma(x) dx$$

- where
- ρ = density of target material
 - M = mass of target atoms
 - $\sigma(x)$ or $\sigma(\theta)$ = cross section for scattering (total) through an angle greater than $\theta = \tan^{-1} \frac{R}{x}$
 - θ = center-of-mass angle
 - ϕ = laboratory-system angle.

Transforming to angular variables,

$$\begin{aligned} \sigma(\theta) &= \int_{\theta}^{\pi/2} 2\pi \sin \theta' \left(\frac{d\sigma}{d\omega} \right)_{\text{c.m.}} d\theta' = 2\pi \cos \theta \overline{\left(\frac{d\sigma}{d\omega} \right)_{\text{c.m.}}} \\ &\cong 2\pi \overline{\left(\frac{d\sigma}{d\omega} \right)_{\text{c.m.}}} \cos 2\phi, \quad \text{since } \theta \cong 2\phi. \end{aligned}$$

But $x = R \cot \phi$, $dx = -R \csc^2 \phi d\phi$,

$$\Delta g = \frac{2\pi\rho R}{M} \overline{\left(\frac{d\sigma}{d\omega} \right)_{\text{c.m.}}} \int_{\phi_1}^{\phi_2} \csc^2 \phi \cos 2\phi d\phi.$$

$$\begin{aligned} \text{Now } \int_{\phi_1}^{\phi_2} \csc^2 \phi \cos 2\phi d\phi &= \int_{\phi_1}^{\phi_2} (\csc^2 \phi - 2) d\phi = - [\cot \phi + 2\phi]_{\phi_1}^{\phi_2} \\ &= \frac{t}{R} - 2(\phi_2 - \phi_1) \quad \text{since } \cot \phi_2 = \frac{L}{R}; \cot \phi_1 = \frac{L+t}{R}, \end{aligned}$$

$$\Delta g = \frac{2\pi\rho t}{M} \overline{\left(\frac{d\sigma}{d\omega} \right)_{\text{c.m.}}} \left[1 - \frac{2R}{t} (\phi_2 - \phi_1) \right].$$

REFERENCES

1. Chamberlain, Segrè, and Wiegand, Phys. Rev. 83, 923 (1951).
2. Kruse, Teem, and Ramsey, Phys. Rev. 94, 1795 (1954).
3. Cassels, Pickavance, and Stafford, Proc. Roy. Soc. (London) A214, 262 (1952).
4. C. L. Oxley and R. D. Schamberger*, Phys. Rev. 85, 416 (1952).
5. O. A. Towler, Jr.,* Phys. Rev. 85, 1024 (1952).
6. Mott, Sutton, Fox, and Kane, Phys. Rev. 90, 712 (1953).
7. Marshall, Marshall, and Nedzel, Phys. Rev. 91, 767 (1953).
8. " " " Phys. Rev. 92, 834 (1953).
9. O. Chamberlain and J. Garrison, Phys. Rev. 95, 1349 (1954).
10. D. Fischer and G. Goldhaber, Phys. Rev. 95, 1350 (1954).
11. Breit and Gluckstern, Annual Review of Nuclear Physics, Vol. 2, Annual Reviews Inc., Stanford, Calif. (1953).
12. R. S. Christian and H. P. Noyes, Phys. Rev. 79, 85 (1950).
13. K. M. Case and A. Pais, Phys. Rev. 80, 203 (1950).
14. Robert Jastrow, Phys. Rev. 81, 165 and 636 (1951).
15. L. J. B. Goldfarb and D. Feldman, Phys. Rev. 88, 1099 (1952).
16. R. S. Christian, Reports on Progress in Physics 15, 68 (1952). (Review Article).
17. D. R. Swanson, Phys. Rev. 89, 740 (1953).
18. H. P. Noyes and H. G. Camnitz, Phys. Rev. 88, 1206 (1953).
19. F. T. Solmitz, Phys. Rev. 92, 164 (1953).
20. A. Garren, Phys. Rev. 92, 213 (1953).
21. R. M. Thaler and J. Bengston, Phys. Rev. 94, 679 (1954).
22. R. M. Thaler, J. Bengston, and G. Breit, Phys. Rev. 94, 683 (1954).
23. Chamberlain, Segrè, Tripp, Wiegand, and Ypsilantis, Phys. Rev. 93, 1430 (1954).
24. H. G. deCarvalho, E. Heiberg, and J. Marshall, Phys. Rev. 94, 1796 (1954).
25. J. M. Dickson and D. C. Salter, Nature 173, 946 (1954).

*The activation cross section for the nuclear reaction $C^{12}(p, pn)C^{13}$, upon which Oxley and Schamberger⁴ and Towler⁵ depend for their absolute calibration has been recently remeasured,³⁰ giving a value of 32.9 ± 1.1 millibarns at 240 Mev. Owing to the method of beta counting used at Rochester, it is uncertain at this time how much the results of Oxley et al, and Towler should be changed, but in any event the corrections will serve to reduce the Rochester values.

26. Chamberlain, Donaldson, Segrè, Tripp, Wiegand, and Ypsilantis, Phys. Rev. 95, 850 (1954).
27. Kane, Stallwood, Sutton, Fields, and Fox, Phys. Rev. 95, 1694 (1954).
28. B. A. Jacobsohn, Phys. Rev. 89, 881 (1953).
29. D. Feldman, Phys. Rev. 89, 1159 (1953).
30. Birnbaum, Millburn, Crandall, and Pyle, $C^{12}(x, xn)C^{11}$ and $Al^{27}(x, x2pn)Na^{24}$ Cross Sections at High Energies, University of California Radiation Laboratory, Report No. UCRL-2756, November 1, 1954.
31. R. L. Garwin, Rev. Sci. Instr. 21, 569 (1950).
32. J. Marshall, private communication to C. Wiegand and O. Chamberlain.
33. O. Chamberlain and C. Wiegand, private communication.
34. Aron, Hoffman, and Williams, AECU-663, Range Energy Curves (UCRL-121 (2nd. rev.)) 1949.
35. L. Wolfenstein and J. Ashkin, Phys. Rev. 85, 947 (1952).
36. A. J. Kirschbaum, Nuclear Absorption Cross Sections for High Energy Protons, University of California Radiation Laboratory, Report No. UCRL-1967, October 1952.
37. C. E. Leith, Phys. Rev. 78, 89 (1950).
38. International Critical Tables (McGraw-Hill Co. 1926), Vol. I, p. 102.
39. B. D. Fried, Phys. Rev. 95, 851 (1954).
40. R. H. Dalitz, Proc. Phys. Soc. A65, 175 (1952).
41. Randle, Taylor, and Wood, Proc. Roy. Soc. A213, 392 (1952).
42. Hadley, Kelly, Leith, Segrè, Wiegand, and York, Phys. Rev. 75, 351 (1949).
43. Guernsey, Mott, and Nelson, Phys. Rev. 88, 15 (1952).
44. Kelley, Leith, Segrè, and Wiegand, Phys. Rev. 79, 96 (1950).
45. Hartzler and Siegel, Phys. Rev. 95, 185 (1954).
46. Garren and Wolfenstein, Unpublished report; we thank the authors for sending us a copy.